

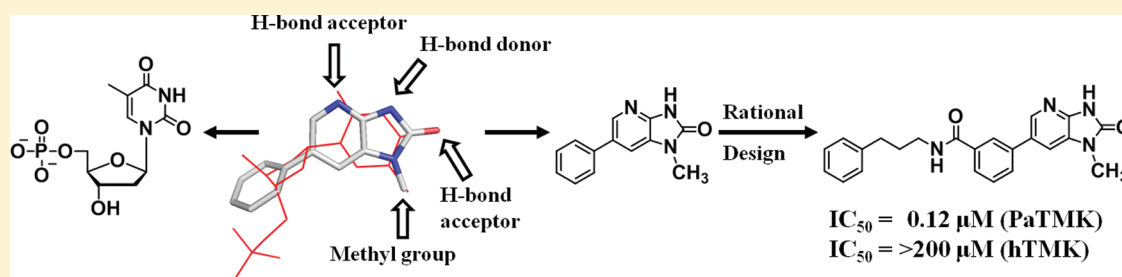
Structure Guided Development of Novel Thymidine Mimetics Targeting *Pseudomonas aeruginosa* Thymidylate Kinase: From Hit to Lead Generation

Jun Yong Choi,[†] Mark S. Plummer,^{*,‡} Jeremy Starr,[‡] Charlene R. Desbonnet,[§] Holly Soutter,^{||} Jeanne Chang,^{||} J. Richard Miller,[§] Keith Dillman,^{||} Alita A. Miller,[§] and William R. Roush^{*,†}

[†]Department of Chemistry, Scripps Florida, Jupiter, Florida 33458, United States

[‡]Antibacterials Medicinal Chemistry, [§]Antibacterials Research Unit, and ^{||}Structural Biology and Biophysics, Pfizer Global Research and Development, Groton, Connecticut 06340, United States

Supporting Information



ABSTRACT: Thymidylate kinase (TMK) is a potential chemotherapeutic target because it is directly involved in the synthesis of an essential component, thymidine triphosphate, in DNA replication. All reported TMK inhibitors are thymidine analogues, which might retard their development as potent therapeutics due to cell permeability and off-target activity against human TMK. A small molecule hit (**1**, $IC_{50} = 58 \mu M$), which has reasonable inhibition potency against *Pseudomonas aeruginosa* TMK (PaTMK), was identified by the analysis of the binding mode of thymidine or TP_5A in a PaTMK homology model. This hit (**1**) was cocrystallized with PaTMK, and several potent PaTMK inhibitors (leads, **46**, **47**, **48**, and **56**, $IC_{50} = 100\text{--}200 \text{ nM}$) were synthesized using computer-aided design approaches including virtual synthesis/screening, which was used to guide the design of inhibitors. The binding mode of the optimized leads in PaTMK overlaps with that of other bacterial TMKs but not with human TMK, which shares few common features with the bacterial enzymes. Therefore, the optimized TMK inhibitors described here should be useful for the development of antibacterial agents targeting TMK without undesired off-target effects. In addition, an inhibition mechanism associated with the LID loop, which mimics the process of phosphate transfer from ATP to dTMP, was proposed based on X-ray cocrystal structures, homology models, and structure–activity relationship results.

INTRODUCTION

Most classes of antibacterial agents currently employed in clinical use were discovered over 45 years ago, with the exception of the oxazolidinone class (Linezolid), introduced in 2000 to treat Gram-positive infections. New antibacterial therapeutics that utilize new mechanisms of action are urgently needed to combat growing resistance to existing antibacterial agents for both Gram-positive and Gram-negative infections. Although the discovery of new antibacterial classes is extraordinarily difficult,¹ the need is especially high for Gram-negative organisms prevalent in the hospital and in particular for infections caused by *Pseudomonas aeruginosa* (Pa), for which treatment options are often limited.^{2–4}

Thymidylate kinase (TMK) has emerged as an attractive therapeutic target because inhibiting TMK functions blocks DNA synthesis in replicating organisms.⁵ TMK phosphorylates thymidine monophosphate (dTMP) to thymidine diphosphate (dTDP), using ATP as a phosphoryl donor.⁶ In addition, TMK

is the last specific enzyme in the pathways for the synthesis of thymidine triphosphate (dTTP), which is an essential component in DNA synthesis.⁷ Therefore, targeting bacterial TMK has been the subject of recent investigation with inhibitors of *Mycobacterium tuberculosis*,^{8–12} *Staphylococcus aureus*,¹³ and *Bacillus anthracis*¹⁴ TMKs reported in conjunction with their cognate protein crystal structures.

However, most of the reported TMK inhibitors are thymidine derived (Figure 1).^{15–21} Although inhibitor design has been enhanced by utilizing protein structures,²¹ computer-aided design,²⁰ and quantitative structure–activity relationship (QSAR) methods,¹⁹ the thymine headgroup of the inhibitors always remains (Figure 1). The thymine headgroup was viewed as a hindrance for designing inhibitors that penetrate the complex cell membrane and avoid efflux pumps prevalent in Pa.

Received: October 8, 2011

Published: January 13, 2012

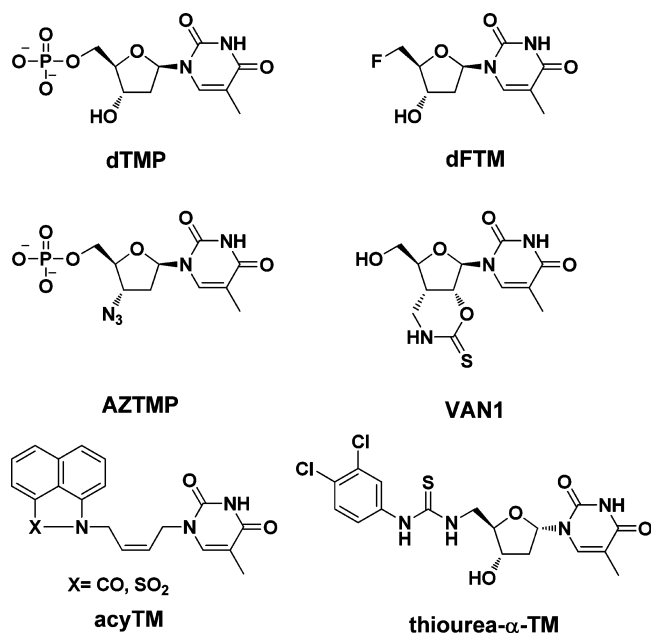


Figure 1. Known TMK inhibitors.

Therefore, small molecule TMK inhibitors, or nonsubstrate analogues, are necessary to develop antibacterial therapeutics. Herein, we report a nonthymidine inhibitor (**1**) targeting PaTMK, the cocrystal structures of **1**, and the evolved inhibitor analogue **17** with PaTMK and structure-guided development of TMK inhibitors. To our knowledge, this is the first report of TMK inhibitors dispossessing the thymidine moiety and its cocrystal structure with PaTMK. In addition, we describe the use of computer-aided design, including virtual synthesis and screening, with the cocrystal structures to expedite rational design and synthesis of more potent PaTMK inhibitors.

RESULTS AND DISCUSSION

Hit Generation. Structural analysis of a PaTMK homology model built based on cocrystal structure (PDB ID: 4TMK) of *Escherichia coli* TMK²² with the thymidine-based dual substrate inhibitor P1-(5'-adenosyl)-P5-(5'-thymidyl)pentaphosphate (TP₅A) led us to intimately understand the interactions required for thymidine binding to its binding site of PaTMK (Figure 2a). Furthermore, we found that a commercial compound, 1-methyl-6-phenyl imidazopyridinone (**1**), has similar chemical properties to thymidine, although their two-dimensional structures have low similarity. Flexible alignment

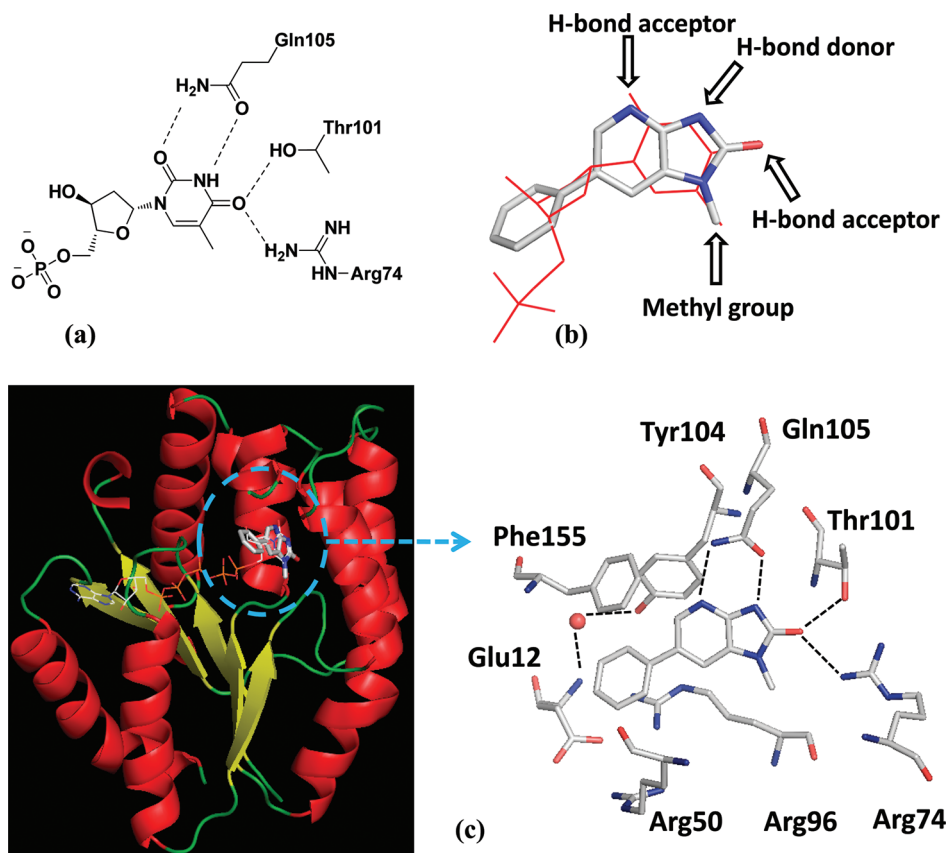
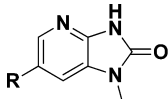
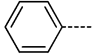
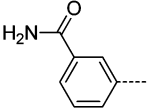
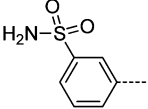
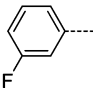
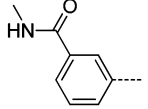
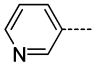
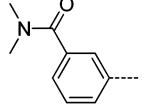
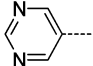
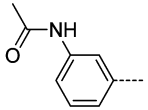
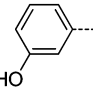
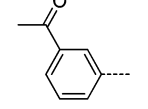
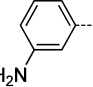
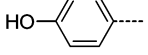
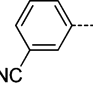
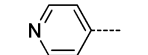
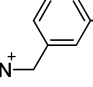
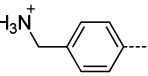
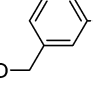
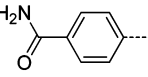


Figure 2. Key interactions of dTMP and **1** in PaTMK. (a) Thymidine interactions in the active site of PaTMK in the homology model are represented in two-dimensional view. (b) The result of flexible alignment of **1** to dTMP shows a clear pharmacophore match between **1** and dTMP. The structure of dTMP is represented as a red line, and that of **1** is as stick with atom type color (gray for carbon, blue for nitrogen, red for oxygen, and orange for phosphorus). (c) The overall X-ray cocrystal structure of PaTMK and **1** shows that **1** binds where dTMP bound (left panel). The structure of TP₅A was merged from the reported X-ray structure (PDB ID: 4TMK) to compare the similarity of the binding site of **1** and TP₅A. The binding mode of **1** in PaTMK at the X-ray cocrystal structure shows that the binding pose of **1** at PaTMK is identical to that of dTMP. The α -helix is red, the β -sheet is yellow, and the loop is green (left panel). The water molecule is represented with a red sphere, **1** and amino acids associated with the binding of **1** are represented as sticks with atom type color, and H-bond interactions are represented with black lines. π -Cation stacking between the phenyl ring of **1** and Arg96 is not marked. Hydrogen atoms are omitted for clarity. Figures are generated with the Pymol program.

Table 1. ^a

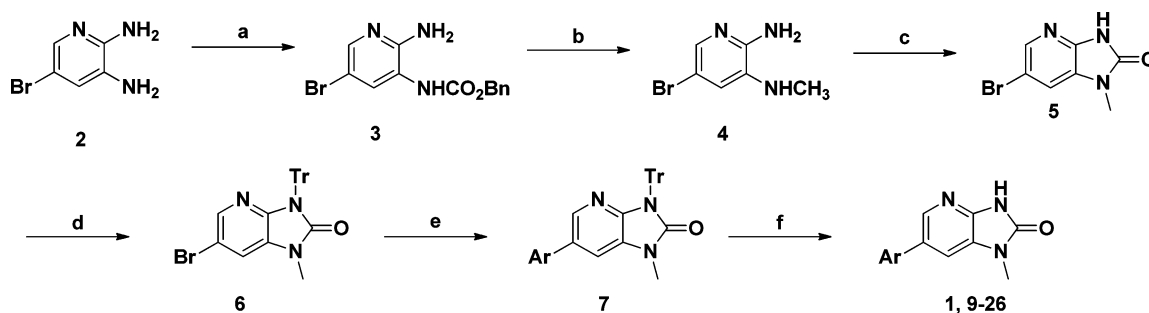
					
Compound	R	IC ₅₀ (μM)	Compound	R	IC ₅₀ (μM)
1		58 ± 11	17		0.44 ± 0.13
dFTM	N/A	20 ± 4	18		>200
9		>200	19		2.2 ± 0.4
10		66 ± 2	20		104
11		>200	21		3.4 ± 0.7
12		11 ± 2	22		13
13		63	23		21
14		>200	24		152
15		>200	25		4.9
16		37 ± 2	26		>200

^aEach reported IC₅₀ was determined at least in duplicate and is an average of the individual values determined. Each individual IC₅₀ value in a single determination was the result of a 20 point IC₅₀ curve with each point determined in duplicate.

of **1** to thymidine structure was performed to recognize their geometrical similarity using the Molecular Operating Environment program (MOE).²³ The result showed that **1** and thymidine are well overlapped with an identical pharmacophore (Figure 2b). In the enzyme assay, compound **1** proved to be an inhibitor of PaTMK with approximately 3-fold less potency than the known TMK inhibitor, deoxy-fluorothymidine (dFTM) (IC₅₀ = 58 μM vs 20 μM in Table 1).

X-ray Structure Analysis. To elucidate the binding mode of **1** to facilitate the structure-based development of TMK inhibitors, **1** was cocrystallized with PaTMK, as described in the Supporting Information, yielding cocrystals that diffracted to 1.91 Å. Gratifyingly, many of the interactions predicted in our homology model and flexible alignment are identical to those in the X-ray cocrystal structure (Figure 2c). Especially important for molecular recognition is the ability of the cyclic

imidazopyridinone functionality to satisfy the hydrogen bond donors and acceptors of the typical thymidine substrate: specifically accepting hydrogen bonds from Arg74 and Thr101, while both donating and accepting hydrogen bonds with Gln105 (Figure 2c). Other important interactions with the distal phenyl ring are the boxlike face to face and edge to face aromatic interactions²⁴ with Phe155 and Tyr104, which are complemented by the π -cation interaction with Arg96.^{25–27} Also apparent is a structural water molecule that bridges between the phenolic –OH group of Tyr104 and the amide backbone (–NH) of Glu12. Although this bridging water does not offer a favorable binding interaction with the inhibitor, it is located only 3.8 Å from the meta-position of the distal phenyl ring. Thus, the bridging structural water suggests a design opportunity for increasing potency via either displacement or additional interaction through hydrogen bonding.²⁸

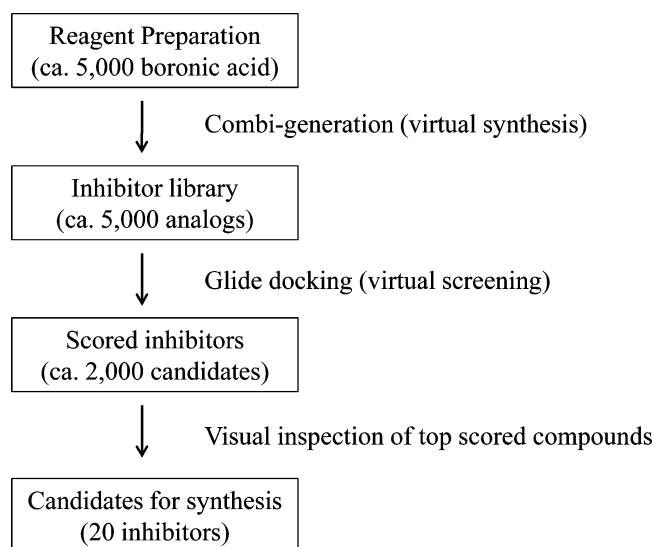
Scheme 1. ^a

^aReagents and conditions: (a) ClCO_2Bn , Pyridine, 0 °C to room temperature, 5 h, 48%. (b) LiAlH_4 , Et_2O , 0 °C to room temperature, 6 h, 99%. (c) Triphosgene, THF, room temperature to reflux, 4 h, 83%. (d) Ph_3CCl , Et_3N , CH_2Cl_2 , room temperature, 1 h, 84%. (e) Aryl boronic acid, 1 mol % $\text{Pd}_2(\text{dba})_3$, 2 mol % PCy_3 , K_3PO_4 , dioxane, 100 °C (microwave), 1 h. (f) TFA, CH_2Cl_2 , room temperature, 30 min, 50–99% (over two steps).

Synthesis of 1 and Its Analogues. The synthesis of analogues of **1** was accomplished using **6** as a key intermediate (Scheme 1). Briefly, 5-bromo 2,3-diaminopyridine **2** was treated with benzyl chloroformate to give benzyl carbamate **3**.²⁹ The urethane was reduced to a methyl group with lithium aluminum hydride, and the diamine was cyclized to the urea **5**, utilizing triphosgene.³⁰ Palladium-mediated coupling reactions of **5** were accomplished efficiently when the acidic urea NH was protected with a trityl group as in **6**. The coupling reaction of **6** with phenyl boronic acid provided **7** in good yield when performed under microwave conditions.^{31–34} Removal of the trityl group with trifluoroacetic acid provided the final inhibitor, **1**. Various aryl boronic acids proposed by computational studies were coupled to the intermediate **6** to produce the first inhibitor library.

Virtual Synthesis/Screening of First Round PaTMK Inhibitors. As described in the analysis of the cocrystal structure, the phenyl ring of **1** can be further modified to increase inhibition potency by replacing it with electron-rich aromatic rings and/or by incorporating functional groups replacing the water molecule near Tyr104. In terms of synthesis, aryl boronic acids can be coupled with intermediate **6** followed by trityl deprotection to produce **1** and its analogues (Scheme 1). Therefore, to increase the diversity of inhibitors being designed, virtual synthesis of inhibitors followed by docking and scoring was applied as outlined in Scheme 2. First, 5000 commercially available boronic acids were computationally attached to the 6-position of imidazopyridine-2-one **5** with the combi-gen program in MOE. The virtually synthesized 5000 compounds were docked into the active site of PaTMK with the water molecule removed using Glide 5.5.³⁵ Hits were ranked and sorted with docking score function ranging from -11.5 to -2.3 kcal/mol. In this virtual screening, the lead inhibitor **1** ranked 1933th with a score of -8.7 kcal/mol. The virtual compounds with scores lower than **1** were visually inspected using the maestro9.0 program;³⁶ most aryl appendages targeted nearby amino acid residues such as the hydroxyl group of Tyr104, the carboxyl groups of Asp153 and Glu156, and the guanidine group of Arg50. About 20 compounds were selected for synthesis, each of which had small aryl groups that offered favorable interactions with the protein, along with polar functionality to generally improve physical properties while preserving the hydrogen-bonding network of the imidazopyridinone. This structure-guided design and synthesis resulted in the discovery of **17** ($\text{IC}_{50} = 0.44 \mu\text{M}$)

Scheme 2



and **19** ($\text{IC}_{50} = 2.2 \mu\text{M}$), which have 130- and 30-fold improved inhibition over **1**, respectively.

Analysis of First Round PaTMK Inhibitors and X-ray Cocrystal Structure of 17 with PaTMK. The tactic of displacing the water molecule near Tyr104 with simple H-bond donors and acceptors was explored using the docking result as a guide. The assay results showed good consistency with the rationale proposed with the X-ray structure and the modeling technique with minor differences. The phenol substitution in **12** provided about a 4-fold increase in potency, while the cyano-group in **14** resulted in loss of activity. Not only was the cyano-compound **14** inactive, it also lacked the H-bond-donating ability of the phenol in **12**; therefore, follow-up focused on incorporating hydrogen bond-donating groups that were larger than the cyano-group. The *meta*-aminomethyl group in **15** was chosen as there are several acidic protein residues in the vicinity of the inhibitor binding site such as Glu12, Glu156, and Asp153. The lack of activity observed for this analogue contrasts with the good potency of *para*-aminomethyl analogue **25**, indicating that the *para*-amino methyl group must extend toward the complementary acidic residues providing a favorable protein–ligand interaction. The similar in size but uncharged *meta*-hydroxymethyl group in **16** provided a $37 \mu\text{M}$ inhibitor, a 2-fold increase in potency over **1**, suggesting that the positive charge in **15** was problematic.

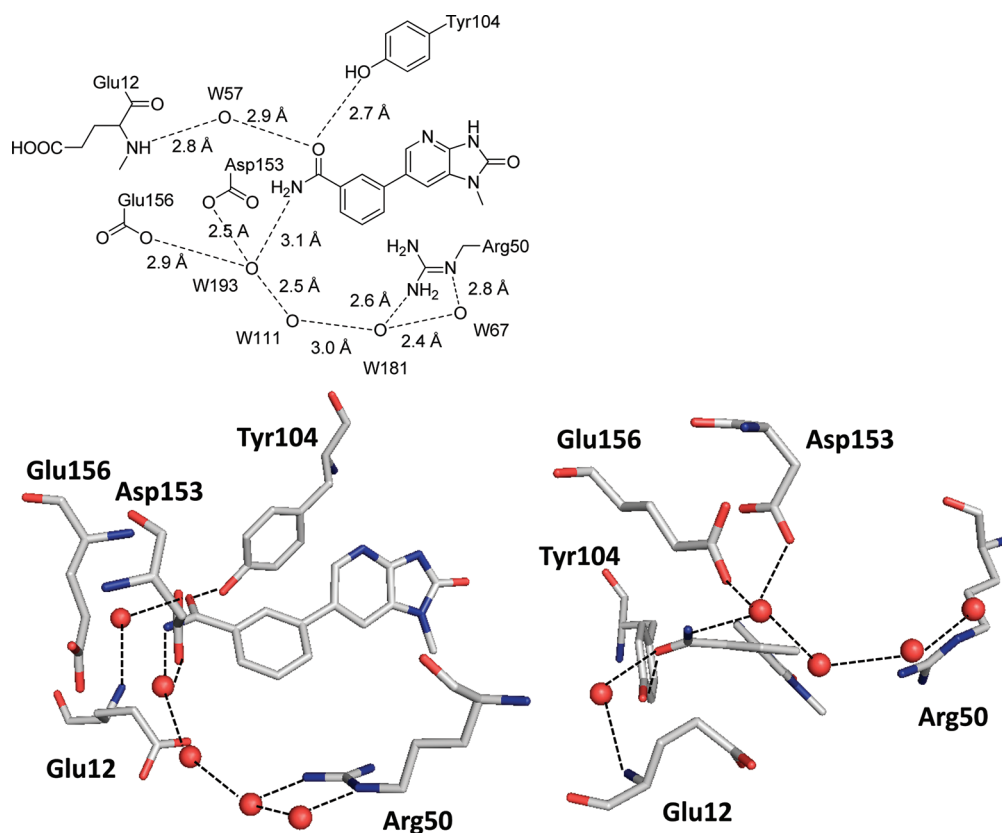
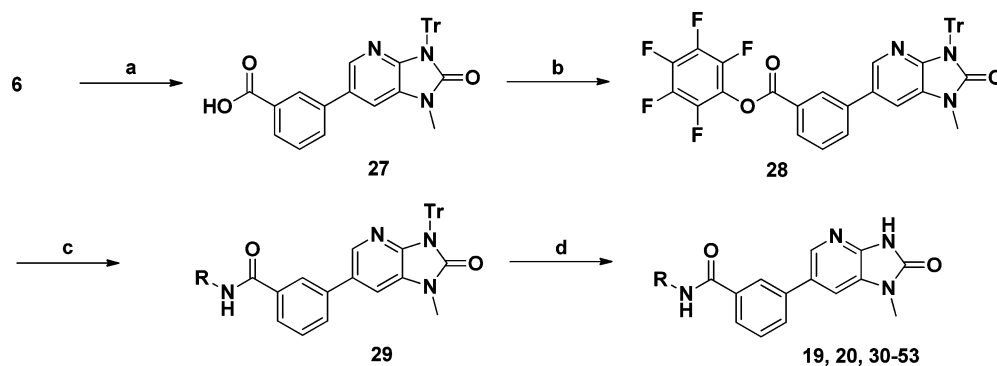


Figure 3. X-ray cocrystal structure of 17 and PaTMK. Key interactions of 17 in the active site of PaTMK are described as 2D (up) and 3D (down) views. For clarity, interactions associated with imidazopyridinone moiety and hydrogen atoms are omitted. Furthermore, water molecules, which are not involved in binding of 17, are omitted. The water molecule is represented as a red sphere, 17 and amino acids are represented as sticks with atom type color, and H-bond interactions are represented with black lines.

Scheme 3.^a

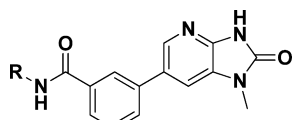


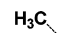
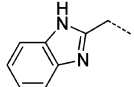
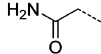
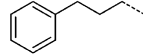
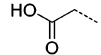
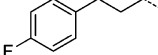
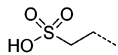
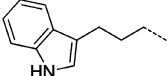
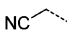
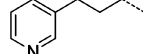
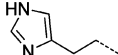
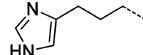
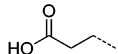
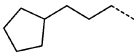
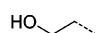
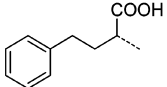
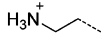
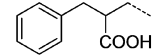
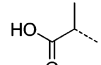
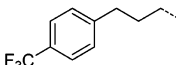
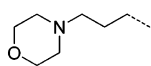
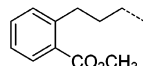
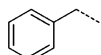
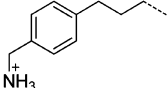
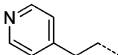
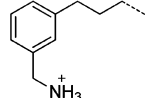
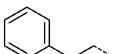
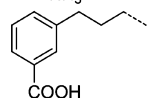
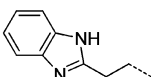
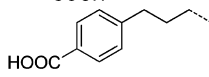
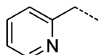
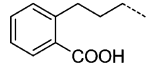
^aReagents and conditions: (a) 3-Carboxyphenylboronic acid, 1 mol % Pd₂(dba)₃, 2 mol % PCy₃, K₃PO₄, dioxane, 100 °C (microwave), 1 h, then aqueous HCl, 99%. (b) Pentafluorophenyl trifluoroacetate, N(*i*-Pr)₂Et, CH₂Cl₂, 0 °C to room temperature, 1 h, 81%. (c) Primary amines, N(*i*-Pr)₂Et, CH₂Cl₂, room temperature, 1 h. (d) TFA, CH₂Cl₂, room temperature, 30 min, 100–56% (over two steps).

In an opposite tactic to displacing the bridging structural water molecule, interactions through this water molecule were probed by incorporation of pyridine, pyrimidine, and fluorine groups as potential hydrogen bond acceptors as in 9–11. Only the pyridine-containing inhibitor 10 retained the meaningful activity of the parent compound 1 (Table 1). As described, the phenyl ring of 1 forms a π -cation interaction with Arg96.^{25–27} Therefore, not surprisingly, compounds with electron-withdrawing groups such as 9, 11, 14, 18, and 26 significantly lost electronic potential at the phenyl ring followed by inhibition potency (IC₅₀ > 200). However, interestingly, 17 has

dramatically increased inhibition potency (130-fold over initial lead 1 and a 60-fold over a standard inhibitor dFTM), although it possesses an electron-poor aryl ring; this is also the case with 19, 21, and 22, which, however, are less potent than 17. These results can be rationalized in the context of the solved X-ray cocrystal structure of 17 and PaTMK (Figure 3).

Inhibitor 17 was cocrystallized with PaTMK and provided a 1.7 Å structure. The binding pose of 17 in virtual synthesis/screening procedure is very consistent with that of the X-ray structure. Indeed, the structural water targeted in the design was clearly displaced with the carboxamide of 17, and a direct

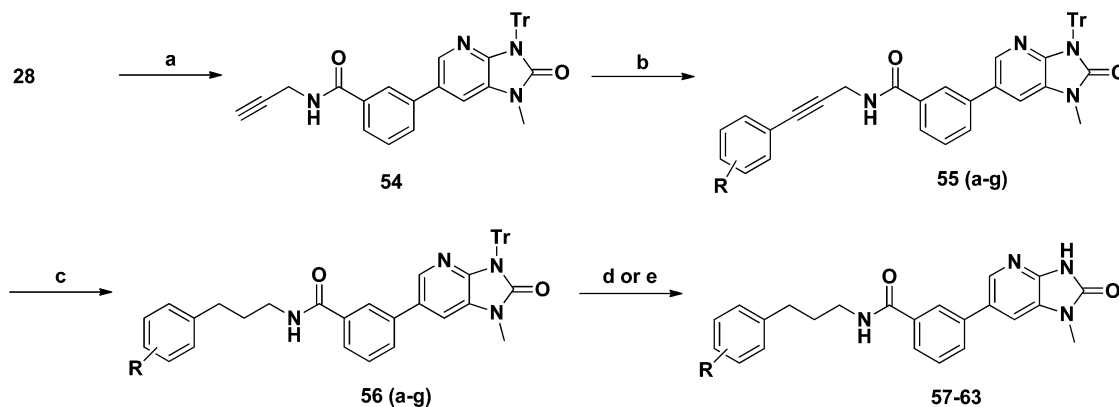
Table 2. ^a


Compound	R	IC ₅₀ (μM)	Compound	R	IC ₅₀ (μM)
19		2.2 ± 0.4	45		68 ± 28
30		0.88 ± 0.31	46		0.12 ± 0.08
31		0.88 ± 0.08	47		0.12 ± 0.05
32		1.3 ± 0.22	48		0.20 ± 0.08
33		2.1 ± 0.3	49		0.51 ± 0.1
34		2.3 ± 0.1	50		0.99 ± 0.14
35		2.6 ± 0.5	51		0.81 ± 0.23
36		2.6 ± 0.2	52		12 ± 2
37		3.2 ± 0.7	53		0.25 ± 0.13
38		5.0	57		0.16 ± 0.05
39		5.8	58		0.37 ± 0.15
40		1.0 ± 0.4	59		3.2
41		2.0 ± 1.0	60		2.2
42		2.9 ± 1.6	61		2.4
43		3.0 ± 1.3	62		2.7
44		6.2 ± 1.6	63		2.0 ± 0.7

^aEach reported IC₅₀ was determined at least in duplicate and is an average of the individual values determined. Each individual IC₅₀ value in a single determination was the result of a 20 point IC₅₀ curve with each point determined in duplicate.

hydrogen bond interaction between the carbonyl oxygen of 17 and the phenolic oxygen of Tyr104 is apparent (Figure 3). Also

present was a water molecule-mediated H-bond network that further hydrates the carboxamide of 17 and could surround the

Scheme 4. ^a

^aReagents and conditions: (a) Monopropargylamine hydrochloride, *N*(*i*-Pr)₂Et, CH₂Cl₂, room temperature to 50 °C, 1 h, 98%. (b) Aryl bromide, 10 mol % Pd(PPh₃)₄, NEt₃, 5 mol % CuI, DMF, 80 °C (microwave), 1 h, 73%. (c) H₂, Pd/C, MeOH, 12 h, 63%. (d) TFA, CH₂Cl₂, room temperature, 30 min, 46%. (e) 10% KOH(aq), MeOH, 60 °C, 12 h, then TFA, CH₂Cl₂, room temperature, 30 min, 22% (over four steps).

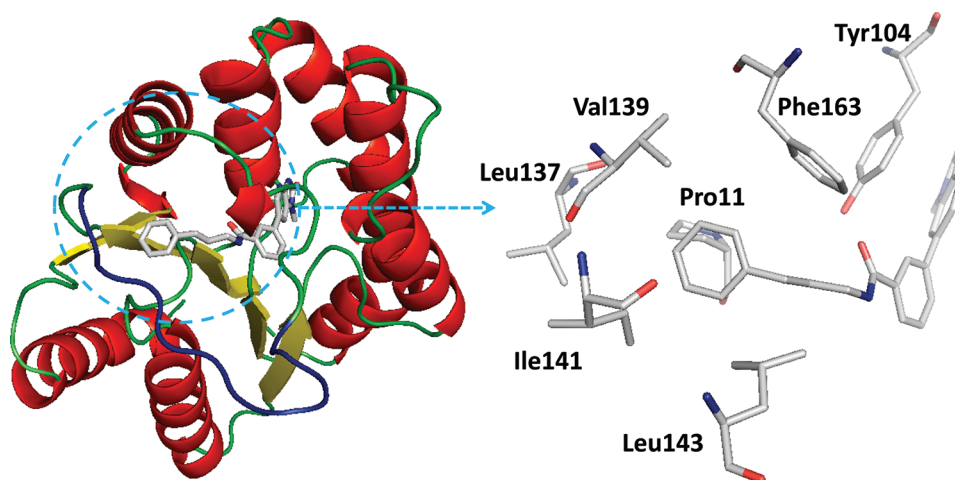


Figure 4. Homology model of PaTMK and **46** based on the X-ray structure of PaTMK and **17**. The blue loop is the generated LID loop in homology modeling. In the close view (right panel), the terminal phenyl ring of **46** occupies the hydrophobic pocket composed of Pro11 (facing to the plane of the phenyl ring), Phe163, Val139, Leu137, Ile141, and Leu143 (surround the terminal phenyl ring of **46**). Other residues in the loop are oriented toward a solvent-accessible area such as Pro138, Glu140, and Gly142, which were omitted for clarity. In addition, interactions associated with imidazopyridinone are the same as those in the previous X-ray cocrystal structure complexed with **1** or **17** as in Figure 2c; thus, these interactions and hydrogen atoms are omitted for a clear view.

entrance of the inhibitor (or dTMP) binding site to make the release of **17** slow. As a combined effect of H-bond interactions with Tyr104 and the H-bond network, PaTMK inhibition by **17** was significantly increased as compared to **1**: ca. 1000-fold increase over **26** (*p*-carboxamide), which possesses an electron-withdrawing group but without the aforementioned cooperative hydrogen-bonding interactions. The effect of the H-bond interactions mediated by a network of water molecules appears to be much more important than H-bond interactions with Tyr104 because of decreased potency of **19** and **20**. The activity of inhibitor **19** (*N*-methylamide), which presumably does not support the extensive H-bond network seen in **17**, was decreased 5-fold as compared with **17**. The importance of the hydrogen bonds with the structural water molecules is supported by the significant, 240-fold decreased inhibition observed for **20** (*N,N*-dimethylamide), which likely would lose the H-bond network while retaining a H-bond interaction with Tyr104. Consequently, as rationalized in the computer-guided design approach, the π -cation interaction of an electron-rich phenyl ring with Arg96 and H-bond interactions of the

carbonyl oxygen of the carboxamide with Tyr104 are important for inhibition of PaTMK. In addition, the X-ray cocrystal structure of **17** provided critical clues, specifically the water-mediated H-bond network, which provides dramatically increased potency of **17**, although possessing an electron-withdrawing group. Because the secondary amide **19** retained reasonable potency and intermediate **28** (Scheme 3) was conducive to rapid analogue production, this vector was explored with the aim of increasing potency.

Virtual Synthesis/Screening of Second Round PaTMK Inhibitors. A second round of virtual synthesis was designed to efficiently expand diversity on lead **19**. Virtual synthesis was performed with 1188 commercially available primary amines to obtain various alkyl-tethered benzamide derivatives that were then virtually screened by docking into the active site of PaTMK using Glide 5.5. About 900 hits were ranked and sorted with docking scores ranging from -14.6 to -0.9 kcal/mol. Among them, inhibitor **19** ranked 390th with a score of -11.4 kcal/mol. With a focus on improving potency, 20 compounds were selected for synthesis by visually inspecting the top-

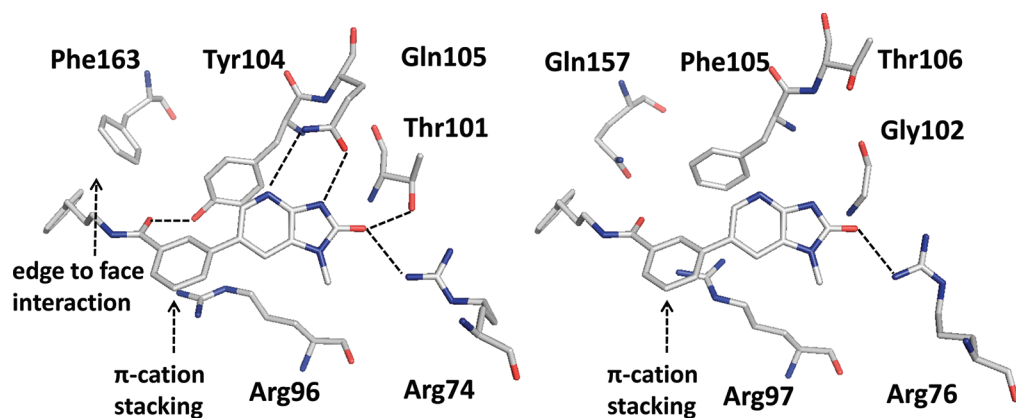


Figure 5. Comparison of the active sites of PaTMK (left) and hTMK (right). Amino acids associated with the interaction of **46** in PaTMK and their corresponding amino acids in hTMK are represented as sticks with atom type color. The structure of **46** and PaTMK was obtained from the docking study with the X-ray cocrystal structure of PaTMK complexed with **17**. The structure of **46** and hTMK was obtained through structure-based multiple sequence alignment followed by merging the coordinate of **46** to hTMK structure (PDB ID: 1E2F) from PaTMK structure. H-bond interactions are highlighted with dashed black lines. Edge to face hydrophobic interactions and π -cation stacking are annotated with black arrows.

scoring compounds followed by ranking for size and enhanced interaction with the protein while maintaining the integrity of the imidazopyridinone hydrogen-bonding interactions (Table 2).

Synthesis of 19 and Its Analogues. Synthesis of analogues of **19** was achieved using **28** as a key intermediate (Scheme 3). Intermediate **6** in Scheme 1 was coupled with 3-carboxyphenylboronic acid to provide **27** in near quantitative yield. The acid in **27** was activated as the pentafluorophenyl ester **28**, which was stable to storage (0.1 M solution of CH_2Cl_2). About 0.2 mmol of **28** (2 mL solution of CH_2Cl_2) was treated with the various primary amines and diisopropylethylamine to provide the desired amides. Removal of the trityl group with TFA provided the final inhibitors. In addition, for modification of the terminal phenyl ring of **46**, intermediate **28** was treated with propargylamine to produce **54** (Scheme 4). The terminal alkyne of **54** was coupled with various aryl bromides mediated by Pd(0) in the presence of a catalytic amount of copper(I) iodide to give **55**. Hydrogenation of **55** provided arylpropyl amides **56** from which the trityl group was removed with TFA to give the desired inhibitors **57–63**.

Assay Results of Second Round PaTMK Inhibitors. A number of small polar secondary amides were synthesized to explore functionality accommodated by the binding pocket **30–38** (Table 2). The glycinamide and glycine analogues **30** and **31** proved to be the most potent polar analogues synthesized. Each has submicromolar activity and improved potency about 2.5-fold over secondary amide **19**, although they were both less potent than the parent amide analogue **17**. Both negatively and positively charged groups as in **31**, **32**, **35**, and **37** also were accommodated without large changes in potency when compared with **19**.

The X-ray cocrystal structure of **17** indicated that the area immediately adjacent to the *m*-carboxamide might also have hydrophobic character (Figure 4), so small hydrophobic extensions of the amide were investigated as in compounds **40–47** (Table 2). Inhibitors **40** and **41** both retained the potency of the parent methylamide **19** showing that larger groups could be accommodated in this area. Because potency did not increase in a manner commensurate with the increase in size, **40** and **41** were deemed inefficient binding ligands. More polar heterocycles as in **43–45** lost potency as compared with **19**, which was in contrast to the glycinamide **30** where a

polar group increased potency. Exploring extension of the hydrophobic group in the series **40** to **42** to **46/47/57** indicated that a propyl spacer between the amide was optimal with inhibitor **46** having 0.12 μM inhibitory activity, an 18-fold improvement over the methyl amide **19**. Inhibitors **47** and **48** both retain a high level of potency, indicating that electronic characteristics and steric bulk can be varied. The addition of polar groups in **59–63** to the phenyl ring resulted in a 4–20-fold loss of inhibition as compared with **46**. Introduction of the carboxyl group into the propyl side chain, making hybrids of **31** and **46** provided racemic compound **52**, lost significant potency. However, the hybrid of **35** and **46** giving racemic inhibitor **53** with a carboxyl group proved to be a useful combination where a good level of potency was retained.

Analysis of Second Round PaTMK Inhibitors. The trend of the second round SAR is that compared to **19**, ca. 18-fold increased potency of inhibitors **46**, **47**, **48**, **53**, and **57**, which possess hydrophobic aromatic rings linked with an aliphatic propyl chain. However, substitution with small functional groups in **30–38** and an aromatic ring linked with a short aliphatic chain in **40–45** did not provide significantly increased inhibition of PaTMK. For rationalization of these results, homology modeling has been performed to fill out the missing amino acids (Val139 to Arg151, a part of the LID loop^{22,37}) in the X-ray cocrystal structure of PaTMK and **17**, because the terminal phenyl ring of **46** is oriented toward the region where the LID loop is involved (Figure 4). Interestingly, the results of the homology modeling showed that the terminal phenyl ring of **46** occupies a hydrophobic pocket composed of residues such as Pro11, Leu137, Val139, Ile141, Leu143, and Phe163. Therefore, the favorable hydrophobic contact between the terminal phenyl ring of **46** and the hydrophobic pocket may be the main reason for the increased potency of **46**. Furthermore, **47**, **57**, and **58** with *p*-fluoro, *p*-trifluoromethyl, and *o*-methoxycarbonyl groups, respectively, have very similar potency to **46**. However, a terminal aryl ring with charged functional groups as in **59–63** lost about 10-fold inhibition potency. The LID loop is not clearly solved in most X-ray structures of TMK because it is highly flexible. However, it is known that this highly adaptable loop undergoes substantial conformational changes to close the ATP and dTMP binding sites when the phosphoryl donor, ATP, binds to the enzyme for phosphoryl transfer. In addition, TP_ζA , which is a phosphoryl

transfer mimetic, has high binding affinity due to LID loop closure ($K_d = 20$ nM).²² Therefore, the LID loop is directly involved in the mechanism of phosphoryl transfer by covering the active site when both ATP and dTMP are bound. On the basis of our structural model and SAR results, it can be proposed that the terminal phenyl ring of **46** forces shielding of the active site by the LID loop via forming direct hydrophobic contacts between the inhibitor and the hydrophobic pocket of PaTMK, resulting in increased binding affinity of **46**.

Biological Evaluation of Inhibitors. Each compound in Tables 1 and 2 was tested against *P. aeruginosa* PA01 and PAO280 (MexABoprM, MexXY, MexZ efflux pump knock out) and were found to have minimum inhibitory concentrations (MICs) >256 μ g/mL. Inhibitors **46** (and also **47/48/57**) have nanomolar enzyme inhibition and have comparable enzyme inhibition to the cellularly active TMKmt inhibitor [5'-deoxy-5'-N-arylthiourea α -thymidine derivatives (thiourea- α -TM) in Figure 1: $K_i = 1.0$ μ M (against TMKmt) and MIC (*M. bovis*) = 25 μ g/mL]. Therefore, lacking cellular activity in an efflux pump knock out strain suggests that penetration of these inhibitors into the cytosol is probably poor due to the complex cell membrane of Gram-negative bacteria.³⁸

Sequence Similarity and Selectivity with Human TMK. Structure-based multiple sequence alignment of PaTMK with other species including human has been performed to elucidate the selectivity of inhibitors over human TMK (21% sequence identity between *P. aeruginosa* and human TMKs). As indicated in Figure 5, the important amino acids directly involved in the binding of **1**, **17**, and **46** at PaTMK are significantly different from those of hTMK:³⁹ Arg74, Arg96, Thr101, Tyr104, Gln105, and Phe163 of PaTMK are equivalent to Arg76, Arg97, Gly102, Phe105, Thr106, and Gln157, respectively. We envisage Arg76 and Arg97 of hTMK, having a weak H-bond interaction with imidazopyridinone moiety and π -cation interaction with the central phenyl ring of **46**. Importantly, the hTMK interactions with **1** are missing key H-bond interactions of imidazopyridinone moiety with Thr101 and Gln105 of PaTMK. In addition, the Phe105 of hTMK corresponds to Tyr104 of PaTMK, which eliminates the phenolic oxygen, which is involved in the potency boosting H-bond interaction with carboxamide oxygen of **17** and **46**. Furthermore, the Gln157 of hTMK matches to Phe163 of PaTMK, which is associated with LID closing and hydrophobic contacts with **46**. Collectively, the inhibitors presented here would be predicted to have reduced activity toward human TMK.

As a verification of this prediction, five compounds **1**, **17**, **46**, **47**, and **57** were assayed toward human TMK. As shown in Table 3, **1** and **17** are inactive toward hTMK even at high

Table 3. Activity of Selected Inhibitors toward hTMK

compd	IC ₅₀ (μ M)	% inhibition at 200 μ M
DTBN	1.53	
1	>200	17
17	>200	12
46	>200	43
47	123	58
57	124	55

concentration (% inhibition at 200 μ M = 17 and 12%, respectively). In addition, **46**, **47**, and **57** possess meaningful inhibition only at very high concentrations (IC₅₀ = >200, 123,

and 124 μ M, and % inhibition of 43, 58, and 55%, respectively, at 200 μ M). Consequently, these inhibitors have over 1000-fold selectivity for PaTMK over hTMK. That **46**, **47**, and **57** exhibit very weak inhibition of hTMK at a high concentration is consistent with the fact that the hydrophobic pocket formed by LID closing is highly conserved between PaTMK and hTMK [the hydrophobic residues of Val14, Leu135, Leu137, Ala140, and Phe146 of hTMK (PDB ID: 1E2F) are oriented toward the area where the terminal phenyl ring of **46**, **47**, or **57** occupies, and these amino acids are at the equivalent positions of Pro11, Leu137, Val139, Ile141, and Leu143 of PaTMK in Figure 4]. Therefore, because of the hydrophobic contacts of the terminal phenyl ring of **46**, **47**, or **57**, these inhibitors are able to inhibit hTMK but only at a high concentration. In addition, these results indirectly support the proposed inhibition mechanism via hydrophobic contacts assisted by LID loop closing.

CONCLUSION

Visual inspection of the binding of the thymidine mimetic TP₃A in a homology model of PaTMK derived from *E. coli* led to the identification of a novel thymidine mimetic, **1**, which had an IC₅₀ of 58 μ M. Inhibitor **1** was cocrystallized with PaTMK to give the first *P. aeruginosa* TMK cocrystal structure. The binding orientation of **1** is identical to what we expected by the modeling approaches. Affinity optimization of **1** using both structure-based design and its directed library build-up provided inhibitors with nanomolar potency (IC₅₀ = ca. 100–200 nM). The SAR results are fully rationalized with the X-ray cocrystal structures and modeling structures. In particular, the water molecule-mediated H-bond network in **17**, which was not recognized in the modeling approach, plays a significant role for high potency toward PaTMK. In addition, LID loop closing mediated by hydrophobic contacts between the terminal phenyl ring of **46** and the hydrophobic pocket of the PaTMK could be the main reason for high inhibition of **46** toward PaTMK.

There have been many reports of TMK inhibitors using thymidine analogues targeting *M. tuberculosis*, *S. aureus*, and *B. anthracis*. Therefore, we anticipate that the lead compounds **1**, **17**, and **46** that we developed and the knowledge from structure-based SAR will be useful for the development of inhibitors targeting the TMKs of these other species because of high sequence identity within the bacterial TMKs. In particular, the amino acids directly involved in interaction of **1**, **17**, or **46** are very similar within the bacterial species but not in human TMK. Therefore, because of the low similarity of the amino acid residues in the active sites of PaTMK and hTMK, particularly the residues associated with inhibitor binding, the inhibitors described here should enable off-target effects to be avoided. Therefore, the present set of inhibitors has great potential as leads for the development of novel antibacterial agents.

Unfortunately, all of the TMK inhibitors described here were inactive against *P. aeruginosa* bacterial strains. The complex cell membrane of *P. aeruginosa* is an effective barrier for preventing cellular activity of these new TMK inhibitors because growth inhibition did not occur even in an efflux pump knockout strain. It has been proposed that quinolones penetrate the outer membrane of Gram-negative bacteria by translocation through the OmpF channel (in case of *P. aeruginosa*, OprD⁴⁰) due to their unique zwitterionic nature;⁴¹ the inner membrane is crossed, and the cytosol is accessed due to the substantial amount of uncharged properties in the zwitterions.⁴² Therefore, incorporating zwitterions into the inhibitors is a plausible next

strategy for penetrating the complex cell membrane of Gram-negative bacteria and to inhibit *P. aeruginosa* bacteria cell growth and division.

EXPERIMENTAL SECTION

Cloning and Expression of *P. aeruginosa* TMK. Pa TMK was subcloned in the pET15b vector (EMD Biosciences) and expressed in *E. coli* BL21 DE3. Cells were grown in 30 L batches using fermentation at 37 °C in LB broth supplemented with 150 mg/L ampicillin. Cells were grown to late log phase, pelleted by centrifugation, and stored at -80 °C.

Purification. Cell pellets were resuspended in lysis buffer (50 mL of 50 mM NaH₂PO₄, 2 mM TCEP, 5 mM imidazole, pH 7.5, and 300 mM NaCl per 10 g cells). One Roche EDTA-free protease inhibitor tablet was added per 50 mL of lysate. The solution was brought up to 0.002% Benzonase and 10 mM MgCl₂ and lysed by sonication on ice. The lysate was clarified by centrifugation at 20200g for 1 h. The clarified lysate was bound to a HisTrap HP (GE Life Sciences) column that had been equilibrated in 50 mM NaH₂PO₄, 2 mM TCEP, 5 mM imidazole, pH 7.5, and 300 mM NaCl. The bound material was washed with 5 column volumes of 50 mM NaH₂PO₄, 2 mM TCEP, 5 mM imidazole, pH 7.5, and 300 mM NaCl followed by 5 column volumes of 50 mM NaH₂PO₄, 2 mM TCEP, 30 mM imidazole, pH 7.5, and 300 mM NaCl. The bound protein was eluted with a gradient of 5–50% 50 mM NaH₂PO₄, 2 mM TCEP, 500 mM imidazole, pH 7.5, and 300 mM NaCl for 20 column volumes followed by 100% 50 mM NaH₂PO₄, 2 mM TCEP, 500 mM imidazole, pH 7.5, and 300 mM NaCl for 10 column volumes. Fractions containing Pa TMK were pooled and dialyzed against 8 L of 25 mM HEPES, pH 7.5, 2 mM TCEP, and 300 mM NaCl overnight at 4 °C. The dialyzed material was concentrated for loading onto a Superdex 200 column (GE Life Sciences) that had been equilibrated with 25 mM HEPES, pH 7.5, 2 mM TCEP, and 300 mM NaCl. Fractions containing Pa TMK were pooled and concentrated to 10 mg/mL for crystallization.

Crystallization. Pa TMK at 10 mg/mL was mixed with 2 mM inhibitor (from a 100 mM stock in DMSO) and incubated on ice for 30 min. The precipitated material was removed by centrifugation at 12000g for 5 min. The 1, dFTM, and 17 complexes were crystallized by hanging drop vapor diffusion. The protein was mixed 1:1 with a reservoir solution containing 30% PEG 4000, 0.2 M MgCl₂, and 0.1 M Tris, pH 7.5–8.5, and incubated at 22 °C. Crystals were prepared for data collection by cryoprotection in a mother liquor solution containing an additional 20% ethylene glycol and flash freezing in liquid nitrogen.

Data Collection. Diffraction data were collected at 100 K by the rotation method (360 frames, 0.5° oscillation per frame) at beamline 17-ID ($\lambda = 1.0 \text{ \AA}$) at the Advance Photon Source. The data were processed with HKL2000.⁴³

Structure Solution and Refinement. The structure of Pa TMK in complex with 1 was solved by molecular replacement at 3 Å resolution using the structure of *S. pneumo* TMK as a search model in Molrep.⁴⁴ Calculation of the Matthew's coefficient indicated that this crystal form contained two molecules in the asymmetric unit. The correlation coefficient and R factor from the molecular replacement solutions indicated that the correct space group was *P*2₁2₁2. Rigid body and restrained refinement were performed in REFMAC⁴⁵ at 3.0 and 1.9 Å, respectively. Five percent of randomly selected reflections was designated as test reflections for use in the free-*R* cross-validation method⁴⁶ and used throughout the refinement. During the refinement, residues that differed in identity between the Pa and the *S. pneumo* enzymes were mutated to Ala and then built into SigmaA-weighted⁴⁷ $|F_o| - |F_c|$ electron density maps contoured at 2 σ using the visualization and model building program Coot.⁴⁸ Compound 1 was modeled into the SigmaA-weighted $|F_o| - |F_c|$ electron density maps contoured at 2 σ . One hundred water molecules and one magnesium atom were added. The model was refined to a final $R_{\text{cryst}}/R_{\text{free}}$ of 19.5/24.2% in REFMAC (Table 1 in the Supporting Information).

The structure of Pa TMK in complex with dFTM was solved by molecular replacement at 3 Å resolution using the structure of Pa

DHFR from the 1 complex as a search model in PHASER.⁴⁹ Calculation of the Matthew's coefficient indicated that this crystal form contained four molecules in the asymmetric unit. The correlation coefficient and R factor from the molecular replacement solutions indicated that the correct space group was *P*2₁. Rigid body and restrained refinement were performed in REFMAC⁴⁵ at 3.0 and 1.9 Å, respectively. Five percent of randomly selected reflections was designated as test reflections for use in the free-*R* cross-validation method⁴⁶ and used throughout the refinement. dFTM was modeled into the SigmaA-weighted⁴⁷ $|F_o| - |F_c|$ electron density maps contoured at 2 σ . Three hundred seventy-seven water molecules and four magnesium atoms were added. The model was refined to a final $R_{\text{cryst}}/R_{\text{free}}$ of 17.5/23.6% in REFMAC (Table 1 in the Supporting Information).

The structure of Pa TMK in complex with 17 was solved by molecular replacement at 3 Å resolution using the structure of Pa DHFR from the 1 complex as a search model in Molrep.⁴⁴ Calculation of the Matthew's coefficient indicated that this crystal form contained two molecules in the asymmetric unit. The correlation coefficient and R factor from the molecular replacement solutions indicated that the correct space group was *P*2. Rigid body and restrained refinement were performed in BUSTER⁵⁰ at 3.0 and 1.7 Å, respectively. Five percent of randomly selected reflections was designated as test reflections for use in the free-*R* cross-validation method⁴⁶ and used throughout the refinement. Compound 17 was modeled into the SigmaA-weighted⁴⁷ $|F_o| - |F_c|$ electron density maps contoured at 2 σ . Two hundred water molecules were added. The model was refined to a final $R_{\text{cryst}}/R_{\text{free}}$ of 19.2/21.2% in BUSTER⁵⁰ (Table 1 in the Supporting Information).

Coordinates and structure factors of PaTMK complexed with 1, 17, and dFTM are available from the Protein Data Bank with accession codes 3UWK, 3UWO, and 3UXM, respectively.

Thymidylate Kinase Kinetic Assay Materials and Methods.⁵¹ TMK catalyzes the phosphorylation of thymidine-5'-monophosphate (dTMP) to form thymidine-5'-diphosphate (dTDP) in both de novo and salvage pathways of dTTP (thymidine-5'-triphosphate) synthesis and is the last unique enzyme in the pathway specific for dTMP. A 384-well enzyme assay was performed in which dTDP production is enzymatically coupled to NADH oxidation. This permits the rate of TMK turnover to be monitored by the decrease in absorbance at 340 nm. The amounts of each coupling enzyme were optimized to ensure that TMK turnover is rate limiting. The assay utilized 40 data points (absorbance readings) over a 20 min time period to calculate the initial rates produced in the presence of compound relative to that of the inhibited (enzyme in the presence of EDTA) and uninhibited controls (enzyme alone).

The assay component consisted of 2 mM adenosine 5'-triphosphate (ATP), 2 mM phosphoenolpyruvate (PEP), 5 U/mL pyruvate kinase (PK), 5 U/mL lactate dehydrogenase (LDH), 1.2 U/mL nucleotide diphosphate kinase (NDP kinase), 0.22 mM (nicotinamide adenine dinucleotide, reduced form (NADH), 54 μ M thymidine-5'-monophosphate (TMP) in 40 mM HEPES, pH 8.0, 80 mM KCl, and 1.6 mM MgCl₂. *P. aeruginosa* TMK enzyme was cloned, expressed, and purified using standard molecular biology techniques and diluted in enzyme diluent buffer containing 25 mM Tris, pH 7.8, 250 mM NaCl, 5% glycerol, 1 mM DTT, and 0.0025% Triton X-100. Test compounds were solvated in 100% DMSO at 30 mM concentration, and 20 1.67-fold serial dilutions starting at a concentration of 200 or 100 μ M (final concentration) were performed in 96-well polypropylene plates. The Biomek FX was used to dilute and spot 5 μ L = solution containing compound in duplicate into Corning #3702 384-well clear flat bottom polystyrene microplates. The 50 μ L reaction was initiated by the addition of 40 nM enzyme, and the oxidation of NADH was monitored for 20 min at 25 °C at absorbance 340 nm using a Molecular Devices Spectramax Plus plate reader. The initial rates from the kinetic time-course absorbance data for duplicates of each compound concentration were exported into an XLfit4 Excel-based plug-in spreadsheet, which allowed curve fitting and statistical analysis to determine IC₅₀ values for each compound tested. Compounds that

resulted in single-digit micromolar potency were retested to confirm activity.

Human Thymidylate Kinase Assay. The Human Thymidylate Kinase Assay Kit Plus (Catalog no. HTMK500KE at Profoldin) was used for measurement of the inhibition IC_{50} values. The kinase assay is based on detection of ADP generated by the kinase reaction in the presence of the kinase substrate dTMP. The total volume of each assay reaction mixture was 50 μ L. In a black 96-well plate, 1 μ L of inhibitor, 27 μ L of H_2O , 5 μ L of 10 \times assay buffer, 2.5 μ L of 1 mM ATP, 2 μ L of 10 mM dTMP, and 2.5 μ L of 1 μ M human thymidylate kinase were mixed. The reaction mixture was incubated at room temperature for 2 min. Then, 5 μ L of 10 \times MUK Reagent A and 5 μ L of 10 \times MUK Reagent B were added. The reaction was incubated at room temperature for 30 min. Finally, 50 μ L of the fluorescence dye was added, and the fluorescence at 535 nm with excitation at 485 nm was measured. The final concentrations were 50 mM Tris-HCl, pH 8.0, 3 mM $MgCl_2$, 0.2 mM EDTA, 0.5 mM DTT, 50 mM NaCl, 0.003% Brij-35, 50 μ M ATP, 400 μ M dTMP, 50 nM human thymidylate kinase, and 0.39–200 μ M inhibitor. Negative controls (no enzyme control): The assay reactions without the kinase were used as negative controls to observe the fluorescence of the compounds at each concentration. The fluorescence reading without the kinase reaction without compound was used as the 100% inhibition value. Assay controls: The assay reactions with the product of the kinase (5 μ M ADP) were used as assay controls to observe the assay interference of the compounds at each concentration. The data from the assay controls were used for correction of the assay values. The percentage inhibition values were calculated from the corrected assay values and used for IC_{50} curve fitting.

Virtual Synthesis/Screening. The in-house cocrystal structure of PaTMK and **1** was initially applied for docking studies. Protein Preparation Wizard in maestro9.0 was employed to refine the structure for Glide docking by deleting unnecessary metals and water molecules followed by optimizing hydrogen-bonding network. After three water molecules near **1** were removed, a grid was generated using default values except constraints such as the aforementioned three H-bond interactions of **1** with Arg74 and Gln105. The structures of commercially available aryl boronic acids (ca. 5000) were obtained from ZINC database. Virtual inhibitors (5000 analogues of **1**) possessing various aryl groups at the 6-position of **5** in Scheme 1 were generated using 'Combigen' in the MOE program package. These were docked into the active site of PaTMK using Glide 5.0 with XP mode and three predefined constraints. The docking results were scored and sorted based on docking scores. The virtual screening results were visually inspected in maestro9.0, and 20 inhibitors were selected for synthesis and screening.

Similarly, the cocrystal structure of PaTMK and **17** was refined using Protein Preparation Wizard in maestro9.0, and a grid was generated for Glide docking. The structures of primary alkyl and aryl amines were obtained from Sigma-Aldrich, Acros, and Maybridge Websites. 'Combigen' in MOE was applied to generate 1188 virtual inhibitors (analogues of **19** in Scheme 3), which were docked into the active site of PaTMK using Glide 5.0. The docking results were scored and visually inspected to select amine reagents for synthesis and screening.

Loop Searching by Homology Modeling. The cocrystal structure of PaTMK with **17** was applied to fill in the missing loop region (Glu140 ~ Gly150). The complete sequence of *P. aeruginosa* TMK was obtained from Uniprot database (ID: Q9HZN8) and aligned to that of the cocrystal structure using blosum62 algorithm and the tree-based build-up method. The final model was obtained by generating 100 intermediates and averaging these intermediates followed by minimization using Amber99 forcefield with 0.1 rms gradient. The coordination of **46** was docked into the final model by superimposing the model and the result of Glide docking.

Synthesis. General Methods. All reaction solvents were purified before use. Dichloromethane, tetrahydrofuran, dimethylformamide, and toluene were purified by passing through a solvent column composed of activated A-1 alumina. All other reagents purchased from commercial suppliers were used as received. All reactions sensitive to

moisture or oxygen were conducted under an argon atmosphere using flame-dried (under vacuum) or oven-dried glassware (overnight). The removal of solvents was accomplished on a rotary evaporator under reduced pressure in the water bath below 35 $^{\circ}C$ followed by using high vacuum pump. Microwave-assisted reactions were performed using a Biotage Initiator microwave reactor.

Proton nuclear magnetic resonance (1H NMR) spectra and carbon 13 (^{13}C) NMR spectra were recorded on a commercial 400 MHz Bruker NMR spectrometer. Chemical shifts are reported in ppm (δ) relative to tetramethylsilane as an internal standard. Coupling constants (J) are reported in hertz (Hz).

Analytical thin-layer chromatography (TLC) was performed on glass plates precoated with a 0.25 mm thickness of silica gel. The TLC plates were visualized with UV light. Column chromatography was performed using a Biotage Isolera flash purification system using Biotage SNAP HP-SIL cartridge (30 μ m silica, 10–100 g size) and SNAP C18 cartridges. Unless noted otherwise, all compounds isolated by chromatography were sufficiently pure by 1H NMR analysis for use in subsequent reactions.

All final compounds were further introduced to high-performance liquid chromatography (HPLC, Varian 1100 series) on a reverse phase ZORBAX Eclipse XDB-C18 column (4.6 mm \times 150 mm, 5 μ m). A linear gradient elution was performed ranging from 2 to 98% CH_3CN and H_2O (containing 0.1% TFA and 1% CH_3CN) at 1.5 mL/min. The purity of all final compounds (typically $\geq 96\%$) was assayed at 254 nm wavelength.

Benzyl (2-Amino-5-bromopyridin-3-yl)carbamate (3). To a solution of 5-bromopyridine-2,3-diamine (8.0 g, 42 mmol) and pyridine (12 mL) in dry THF (200 mL) was added benzyl chloroformate (11 mL) using a syringe pump (rate 2 mL/h) at 0 $^{\circ}C$. After the addition of benzyl chloroformate was complete, the reaction mixture was stirred at room temperature for 12 h. The excess of ethyl acetate was added to the crude mixture, which was washed with saturated aqueous $NaHCO_3$ and brine. The organic layer was dried over magnesium sulfate, filtered, and concentrated in vacuo. Purification of the crude product by flash chromatography eluting with a linear gradient ranging from 12 to 100% EtOAc–hexane provided 6.6 g (48%) of **3** as a yellow solid. 1H NMR (400 MHz, $DMSO-d_6$): δ 9.00 (s, 1H), 7.90 (s, 1H), 7.80 (d, $J = 2.0$ Hz, 1H), 7.45–7.32 (m, 5H), 6.11 (s, 2H), 5.17 (s, 2H). ^{13}C NMR (100 MHz, $DMSO-d_6$): δ 154.03, 151.04, 142.76, 136.32, 128.45, 128.16, 128.11, 120.16, 104.65, 66.29. MS (ESI) 322, 324 m/z [$M + H$] $^+$.

5-Bromo-N3-methylpyridine-2,3-diamine (4). To a solution of $LiAlH_4$ (3.2 g) in dry ether was added **3** (6.6 g, 20 mmol) at 0 $^{\circ}C$. The reaction mixture was stirred for 15 min, then was warmed to ambient temperature, and stirred for 18 h. The mixture was cooled to 0 $^{\circ}C$, and then, 3.2 mL of water, 3.2 mL of 10% $NaOH(aq)$, and 3.2 mL of water were sequentially added. The precipitated white solid was filtered off, and the filtrate was concentrated with a rotary evaporator. The crude product was purified by flash chromatography eluting with a linear gradient ranging from 12 to 100% EtOAc–hexane yielded 4.1 g (99%) of **4** as a white solid. 1H NMR (400 MHz, $DMSO-d_6$): δ 7.28 (d, $J = 2.4$ Hz, 1H), 6.56 (d, $J = 2.0$ Hz, 1H), 5.64 (s, 2H), 5.22 (d, $J = 4.8$ Hz, 1H), 2.69 (d, $J = 4.8$ Hz, 3H). ^{13}C NMR (100 MHz, $DMSO-d_6$): δ 147.35, 133.47, 133.01, 114.06, 107.14, 29.49. MS (ESI) 202, 204 m/z [$M + H$] $^+$.

6-Bromo-1-methyl-1H-imidazo[4,5-b]pyridin-2(3H)-one (5). To a solution of triphosgene (27 g) in dry toluene (200 mL) was added a solution of **4** (10 g, 50 mmol) in dry THF (20 mL) dropwise at room temperature. The reaction mixture was stirred at 100 $^{\circ}C$ for 5 h. The solution was cooled to ambient, and then, the solvent was removed under reduced pressure. Ethyl acetate and 10% $NaOH(aq)$ were added to the product mixture. The aqueous layer was collected and treated with 1 N $HCl(aq)$ to neutralize it, and a yellow solid was formed. The product was obtained by filtering, and further purification by flash chromatography eluting with a linear gradient ranging from 16 to 100% EtOAc–hexane yielded **5** (9.2 g, 80%) as a yellow solid. 1H NMR (400 MHz, $DMSO-d_6$): δ 11.71 (s, 1H), 7.96 (d, $J = 2.0$ Hz, 1H), 7.70 (d, $J = 2.0$ Hz, 1H), 3.27 (s, 3H). ^{13}C NMR (100 MHz, $DMSO-d_6$): δ 153.79, 142.53, 139.57, 126.42, 116.18, 111.32, 26.50.

MS (ESI) 228, 230 m/z $[M + H]^+$. HRMS (ESI) calcd for $C_7H_7BrN_3O$ $[M + H]^+$, 227.9772; found, 227.9773.

6-Bromo-1-methyl-3-trityl-1H-imidazo[4,5-b]pyridin-2(3H)-one (6). To a solution of **5** (9.2 g, 40 mmol) in dry CH_2Cl_2 (150 mL) were added trityl chloride (13 g, 46 mmol) and NEt_3 (10 mL) at room temperature. The reaction mixture was stirred overnight (ca. 16 h), and the solvent was removed under reduced pressure. The product mixture was diluted with ethyl acetate and washed with saturated $NaHCO_3(aq)$ and brine. The organic layer was dried over magnesium sulfate, filtered, and concentrated in vacuo. Purification of the crude product by flash chromatography eluting with a linear gradient ranging from 6 to 50% EtOAc–hexane provided 17 g (88%) of **6** as a white solid. 1H NMR (400 MHz, $CDCl_3$): δ 7.91 (d, $J = 2.0$ Hz, 1H), 7.63 (d, $J = 7.6$ Hz, 6H), 7.32 (t, $J = 7.4$ Hz, 6H), 7.23 (t, $J = 7.4$ Hz, 3H), 7.17 (d, $J = 2.0$ Hz, 1H), 3.26 (s, 3H). ^{13}C NMR (100 MHz, $CDCl_3$): δ 153.68, 142.52, 139.80, 129.03, 127.38, 126.62, 125.94, 115.20, 112.72, 74.84, 26.88. MS (ESI) 243 m/z [decomposition of trityl group, $M + H]^+$. HRMS (ESI) calcd for $C_{26}H_{21}BrN_3O$ $[M + H]^+$, 470.0868; found, 470.0876.

General Procedure A for Synthesis of Aryl-Substituted Analogues (1 and 9–26) in Scheme 1. **1-Methyl-6-phenyl-3-trityl-1H-imidazo[4,5-b]pyridin-2(3H)-one (7).** A reaction mixture of **6** (0.11 g, 0.23 mmol), phenyl boronic acid (36 mg, 0.30 mmol), $Pd_2(dba)_3$ (5 mg, 2 mol %), PCy_3 (5 mg, 5 mol %), and K_3PO_4 (1 M, 1 mL) in dioxane (4 mL) was stirred under microwave heating (100 °C) for 1 h. The palladium catalyst was removed by filtration. The product mixture was diluted with ethyl acetate (30 mL) and washed with water (10 mL) and brine (10 mL). The organic layer was dried over magnesium sulfate, filtered, and concentrated in vacuo. The resulting product was purified by flash chromatography eluting with a linear gradient ranging from 6 to 50% EtOAc–hexane to afford **7** (0.12 g) as a yellow solid. 1H NMR (400 MHz, $CDCl_3$): δ 7.91 (d, $J = 2.0$ Hz, 1H), 7.46–7.44 (m, 6H), 7.41–7.39 (m, 2H), 7.33–7.30 (m, 2H), 7.23 (t, $J = 7.2$ Hz, 1H), 7.17–7.06 (m, 10H), 3.25 (s, 3H). ^{13}C NMR (100 MHz, $CDCl_3$): δ 154.37, 143.50, 142.99, 138.58, 138.41, 130.72, 129.35, 129.13, 127.62, 127.48, 127.12, 126.69, 125.26, 111.29, 74.91, 27.04. MS (ESI) 243 m/z [decomposition of trityl group, $M + H]^+$. HRMS (ESI) calcd for $C_{32}H_{26}N_3O$ $[M + H]^+$, 468.2076; found, 468.2090.

1-Methyl-6-phenyl-1H-imidazo[4,5-b]pyridin-2(3H)-one (1). To a solution of **7** (0.12 g) in CH_2Cl_2 (5 mL) was added trifluoroacetic acid (1 mL) at room temperature. The reaction mixture was stirred for 30 min. The solvent and trifluoroacetic acid were removed in vacuo. The product **8** was purified by flash chromatography eluting with a linear gradient ranging from 12 to 100% EtOAc–hexane as a white solid (49 mg, 93% over 2 steps). 1H NMR (400 MHz, $DMSO-d_6$): δ 11.58 (s, 1H), 8.21 (d, $J = 2.0$ Hz, 1H), 7.74 (d, $J = 2.0$ Hz, 1H), 7.72–7.69 (m, 2H), 7.48 (t, $J = 7.6$ Hz, 2H), 7.37 (tt, $J = 7.4, 1.2$ Hz, 1H), 3.36 (s, 3H). ^{13}C NMR (100 MHz, $DMSO-d_6$): δ 154.09, 143.09, 138.05, 129.49, 128.95, 127.27, 126.65, 125.40, 112.21, 26.39. MS (ESI) 226 m/z $[M + H]^+$. HRMS (ESI) calcd for $C_{13}H_{12}N_3O$ $[M + H]^+$, 226.0980; found, 226.0981. Purity ($\geq 98\%$, $t_r = 6.58$ min).

6-(3-Fluorophenyl)-1-methyl-1H-imidazo[4,5-b]pyridin-2(3H)-one (9). The general procedure A was followed using **6** (185 mg, 393 μ mol) and 3-fluorophenylboronic acid to give **9** as a white solid (76 mg, 314 μ mol, 80%). 1H NMR (400 MHz, $DMSO-d_6$): δ 11.65 (s, 1H), 8.26 (d, $J = 2.0$ Hz, 1H), 7.79 (d, $J = 2.0$ Hz, 1H), 7.59–7.55 (m, 2H), 7.52–7.46 (m, 1H), 7.18 (tdd, $J = 8.4, 2.4, 1.2$ Hz, 1H), 3.35 (s, 3H). ^{13}C NMR (100 MHz, $DMSO-d_6$): δ 163.93, 161.51, 154.10, 143.52, 140.57, 140.49, 138.26, 130.90, 125.43, 122.60, 122.57, 114.03, 113.82, 113.40, 113.18, 112.23, 26.44. MS (ESI) 244.2 m/z $[M + H]^+$. Purity (96%, $t_r = 6.85$ min).

1-Methyl-6-(pyridin-3-yl)-1H-imidazo[4,5-b]pyridin-2(3H)-one (10). The general procedure was followed using **6** (194 mg, 412 μ mol) and pyridine-3-boronic acid to provide **13** as a white solid (97 mg, 431 μ mol, 100%). 1H NMR (400 MHz, $DMSO-d_6$): δ 11.69 (s, 1H), 8.98 (d, $J = 1.6$ Hz, 1H), 8.61 (d, $J = 3.6$ Hz, 1H), 8.29 (d, $J = 2.0$ Hz, 1H), 8.21 (dt, $J = 4.0, 2.4$ Hz, 1H), 7.86 (d, $J = 2.0$ Hz, 1H), 7.57 (dd, $J = 8.0, 4.8$ Hz, 1H), 3.36 (s, 3H). ^{13}C NMR (100 MHz, $DMSO-d_6$): δ 154.06, 147.41, 146.64, 143.73, 138.34, 134.98, 134.03, 125.97, 125.54,

124.23, 112.20, 26.47. MS (ESI) 227.3 m/z $[M + H]^+$. Purity ($\geq 98\%$, $t_r = 3.74$ min).

1-Methyl-6-(pyrimidin-5-yl)-1H-imidazo[4,5-b]pyridin-2(3H)-one (11). The general procedure A was followed using **6** (202 mg, 431 μ mol) and pyrimidine-5-boronic acid to provide **11** as a yellow solid (78 mg, 346 μ mol, 80%). 1H NMR (400 MHz, $DMSO-d_6$): δ 11.75 (s, 1H), 9.19–9.18 (m, 3H), 8.36 (d, $J = 2.0$ Hz, 1H), 7.94 (d, $J = 2.0$ Hz, 1H), 3.35 (s, 3H). ^{13}C NMR (100 MHz, $DMSO-d_6$): δ 157.07, 154.47, 154.02, 144.11, 138.37, 131.49, 125.61, 123.03, 111.99, 26.52. MS (ESI) 228.4 m/z $[M + H]^+$. Purity ($\geq 98\%$, $t_r = 4.48$ min).

6-(3-Hydroxyphenyl)-1-methyl-1H-imidazo[4,5-b]pyridin-2(3H)-one (12). The general procedure A was followed using **6** (192 mg, 408 μ mol) and 3-hydroxyphenylboronic acid to provide **12** as a dime yellow solid (66 mg, 247 μ mol, 67%). 1H NMR (400 MHz, $DMSO-d_6$): δ 11.58 (s, 1H), 9.68 (br, 1H), 8.13 (d, $J = 2.0$ Hz, 1H), 7.66 (d, $J = 1.6$ Hz, 1H), 7.25 (t, $J = 7.8$ Hz, 1H), 7.09–7.06 (m, 2H), 6.78 (ddd, $J = 8.0, 2.0, 0.8$ Hz, 1H), 3.34 (s, 3H). ^{13}C NMR (100 MHz, $DMSO-d_6$): δ 158.02, 154.19, 143.13, 139.49, 137.98, 129.99, 129.79, 125.42, 117.45, 114.39, 113.63, 112.25, 105.86, 26.43. MS (ESI) 242.2 m/z $[M + H]^+$. Purity (96%, $t_r = 5.48$ min).

6-(3-Aminophenyl)-1-methyl-1H-imidazo[4,5-b]pyridin-2(3H)-one (13). The general procedure A was followed using **6** (121 mg, 255 μ mol) and 3-aminobenzeneboronic acid to provide **13** as a yellow solid (61 mg, 254 μ mol, 100%). 1H NMR (400 MHz, $DMSO-d_6$): δ 11.71 (s, 1H), 10.46 (br, 2H), 8.19 (d, $J = 2.0$ Hz, 1H), 7.75–7.72 (m, 2H), 7.68 (d, $J = 1.6$ Hz, 1H), 7.59 (t, $J = 8.0$ Hz, 1H), 7.38 (dd, $J = 8.0, 1.2$ Hz, 1H), 3.36 (s, 3H). ^{13}C NMR (100 MHz, $DMSO-d_6$): δ 154.08, 143.55, 139.56, 137.98, 133.16, 130.38, 128.24, 126.16, 125.56, 121.96, 121.09, 112.15, 26.45. MS (ESI) 241.2 m/z $[M + H]^+$. Purity ($\geq 98\%$, $t_r = 4.25$ min).

3-(1-Methyl-2-oxo-2,3-dihydro-1H-imidazo[4,5-b]pyridin-6-yl)-benzotrile (14). The general procedure A was followed using **6** (480 mg, 1.02 mmol) and 3-cyanophenylboronic acid to provide **14** as a white solid (265 mg, 537 μ mol, 53%). 1H NMR (400 MHz, $DMSO-d_6$): δ 11.68 (s, 1H), 8.31 (d, $J = 2.0$ Hz, 1H), 8.22 (t, $J = 1.6$ Hz, 1H), 8.08 (ddd, $J = 8.0, 2.0, 1.2$ Hz, 1H), 7.88 (d, $J = 2.0$ Hz, 1H), 7.82 (dt, $J = 8.0, 1.2$ Hz, 1H), 7.67 (t, $J = 8.0$ Hz, 1H), 3.36 (s, 3H). ^{13}C NMR (100 MHz, $DMSO-d_6$): δ 154.10, 143.75, 139.23, 138.41, 131.24, 130.79, 130.15, 130.07, 127.28, 125.51, 118.79, 112.27, 112.14, 26.47. MS (ESI) 251.1 m/z $[M + H]^+$. Purity ($\geq 98\%$, $t_r = 6.32$ min).

6-(3-(Aminomethyl)phenyl)-1-methyl-1H-imidazo[4,5-b]pyridin-2(3H)-one Hydrochloride (15). The general procedure A was followed using **6** (790 mg, 1.66 mmol) and 3-N-Boc-aminomethylphenylboronic acid (0.88 g, 3.09 mmol) to provide **15** as a white solid (0.23 mg, 0.791 mmol, 48%). 1H NMR (400 MHz, D_2O): δ 7.85 (d, $J = 2.0$ Hz, 1H), 7.39–7.26 (m, 4H), 7.15 (d, $J = 1.6$ Hz, 1H), 4.11 (s, 2H), 3.06 (s, 3H), ^{13}C NMR (100 MHz, D_2O): δ 154.92, 141.02, 137.70, 136.97, 133.13, 129.65, 129.13, 127.74, 126.43, 125.99, 124.79, 112.94, 42.92, 26.09. MS (ESI) 255 m/z $[M + H]^+$, Purity ($\geq 98\%$, $t_r = 4.50$ min).

6-(3-(Hydroxymethyl)phenyl)-1-methyl-1H-imidazo[4,5-b]pyridin-2(3H)-one (16). The general procedure A was followed using **6** (127 mg, 270 μ mol) and 3-(hydroxymethyl)phenylboronic acid to provide **16** as a white solid (44 mg, 170 μ mol, 63%). 1H NMR (400 MHz, $CDCl_3$): δ 11.25 (br, 1H), 8.28 (d, $J = 1.2$ Hz, 1H), 7.57–7.33 (m, 5H), 5.41 (s, 2H), 3.46 (s, 3H). ^{13}C NMR (100 MHz, $CDCl_3$): δ 154.84, 143.42, 139.06, 139.06, 134.38, 130.63, 129.88, 128.26, 128.05, 127.62, 126.01, 112.71, 69.57, 26.98. MS (ESI) 256.4 m/z $[M + H]^+$. Purity (95%, $t_r = 5.35$ min).

3-(1-Methyl-2-oxo-2,3-dihydro-1H-imidazo[4,5-b]pyridin-6-yl)-benzamide (17). The general procedure A was followed using **6** (208 mg, 443 μ mol) and 3-carbamoylphenylboronic acid to provide **17** as a white solid (51 mg, 190 μ mol, 43%). 1H NMR (400 MHz, $DMSO-d_6$): δ 11.63 (s, 1H), 8.30 (d, $J = 2.0$ Hz, 1H), 8.18 (t, $J = 1.6$ Hz, 1H), 8.09 (br, 1H), 7.87 (t, $J = 1.6$ Hz, 1H), 7.85 (t, $J = 2.0$ Hz, 1H), 7.81 (d, $J = 2.0$ Hz, 1H), 7.55 (t, $J = 2.0$ Hz, 1H), 7.45 (br, 1H), 3.37 (s, 3H). ^{13}C NMR (100 MHz, $DMSO-d_6$): δ 167.72, 154.09, 143.30, 138.26, 138.01, 135.01, 129.31, 128.95, 128.90, 126.42, 125.51, 125.45, 112.21, 26.42. MS (ESI) 269.1 m/z $[M + H]^+$. HRMS (ESI) calcd for $C_{14}H_{13}N_4O_2$ $[M + H]^+$, 269.1039; found, 269.1041. Purity ($\geq 98\%$, $t_r = 5.00$ min).

3-(1-Methyl-2-oxo-2,3-dihydro-1H-imidazo[4,5-b]pyridin-6-yl)-benzenesulfonamide (**18**). The general procedure A was followed using **6** (233 mg, 490 μ mol) and benzenesulfonamide-3-boronic acid pinacol ester to provide **18** as a white solid (18 mg, 59 μ mol, 12%). ^1H NMR (400 MHz, DMSO- d_6): δ 11.69 (s, 1H), 8.26 (d, J = 2.0 Hz, 1H), 8.15 (t, J = 1.6 Hz, 1H), 7.94 (ddd, J = 7.6, 1.6, 0.8 Hz, 1H), 7.82 (ddd, J = 8.0, 1.6, 1.2 Hz, 1H), 7.77 (d, J = 2.0 Hz, 1H), 7.67 (t, J = 7.6 Hz, 1H), 7.41 (br, 2H), 3.37 (s, 3H). ^{13}C NMR (100 MHz, DMSO- d_6): δ 154.11, 144.91, 143.65, 138.84, 138.25, 129.92, 129.69, 128.18, 125.56, 124.24, 123.59, 112.08, 26.47. MS (ESI) 305.1 m/z [$M + H$] $^+$. Purity ($\geq 98\%$, t_r = 5.07 min).

N-(3-(1-Methyl-2-oxo-2,3-dihydro-1H-imidazo[4,5-b]pyridin-6-yl)phenyl)acetamide (**21**). The general procedure A was followed using **6** (487 mg, 1.04 mmol) and 3-acetamidophenylboronic acid to provide **21** as a yellow solid (105 mg, 373 μ mol, 36%). ^1H NMR (400 MHz, DMSO- d_6): δ 11.63 (s, 1H), 10.04 (s, 1H), 8.13 (d, J = 2.0 Hz, 1H), 7.86 (s, 1H), 7.65 (d, J = 1.6 Hz, 1H), 7.59 (d, J = 7.6 Hz, 1H), 7.41–7.33 (m, 2H), 3.35 (s, 3H), 2.06 (s, 3H). ^{13}C NMR (100 MHz, DMSO- d_6): δ 168.43, 154.10, 143.16, 139.90, 138.58, 137.89, 129.64, 129.35, 125.44, 121.56, 118.00, 117.29, 112.16, 26.39, 24.04. MS (ESI) 283.2 m/z [$M + H$] $^+$. Purity (98%, t_r = 5.44 min).

6-(3-Acetylphenyl)-1-methyl-1H-imidazo[4,5-b]pyridin-2(3H)-one (**22**). The general procedure A was followed using **6** (82 mg, 161 μ mol) and 3-acetylphenylboronic acid to provide **22** as a white solid (29 mg, 108 μ mol, 67%). ^1H NMR (400 MHz, DMSO- d_6): δ 11.64 (s, 1H), 8.29 (d, J = 2.0 Hz, 1H), 8.22 (t, J = 1.6 Hz, 1H), 7.98–7.93 (m, 2H), 7.83 (d, J = 2.0 Hz, 1H), 7.63 (t, J = 8.0 Hz, 1H), 3.37 (s, 3H), 2.70 (s, 3H). ^{13}C NMR (100 MHz, DMSO- d_6): δ 198.00, 154.09, 143.41, 138.54, 138.32, 137.56, 131.29, 129.38, 128.66, 126.91, 126.31, 125.46, 112.32, 26.95, 26.47. MS (ESI) 288.2 m/z [$M + H$] $^+$. Purity ($\geq 98\%$, t_r = 6.19 min).

6-(4-Hydroxyphenyl)-1-methyl-1H-imidazo[4,5-b]pyridin-2(3H)-one (**23**). The general procedure A was followed using **6** (205 mg, 430 μ mol) and 4-hydroxyphenylboronic acid to provide **23** as a dark yellow solid (12 mg, 52 μ mol, 12%). ^1H NMR (400 MHz, DMSO- d_6): δ 11.49 (s, 1H), 9.53 (s, 1H), 8.11 (d, J = 2.0 Hz, 1H), 7.63 (d, J = 2.0 Hz, 1H), 7.50 (dt, J = 8.8, 2.0 Hz, 2H), 6.85 (dt, J = 8.4, 2.0 Hz, 2H), 3.36 (s, 3H). ^{13}C NMR (100 MHz, DMSO- d_6): δ 156.98, 154.08, 142.34, 137.36, 129.70, 128.77, 127.75, 125.31, 115.75, 111.73, 26.33. MS (ESI) 242.2 m/z [$M + H$] $^+$. Purity ($\geq 98\%$, t_r = 5.17 min).

1-Methyl-6-(pyridin-4-yl)-1H-imidazo[4,5-b]pyridin-2(3H)-one (**24**). The general procedure A was followed using **6** (149 mg, 317 μ mol) and pyridine-4-boronic acid to provide **24** as a light yellow solid (56 mg, 246 μ mol, 78%). ^1H NMR (400 MHz, DMSO- d_6): δ 11.81 (s, 1H), 8.71 (s, 2H), 8.47 (d, J = 2.0 Hz, 1H), 7.97 (d, J = 2.0 Hz, 1H), 7.95 (d, J = 6.0 Hz, 2H), 3.37 (s, 3H). ^{13}C NMR (100 MHz, DMSO- d_6): δ 154.06, 148.23, 147.26, 144.84, 139.10, 125.65, 125.58, 121.39, 112.00, 26.53. MS (ESI) 227.2 m/z [$M + H$] $^+$. Purity ($\geq 98\%$, t_r = 3.80 min).

6-(4-(Aminomethyl)phenyl)-1-methyl-1H-imidazo[4,5-b]pyridin-2(3H)-one Hydrochloride (**25**). The general procedure A was followed using **6** (613 mg, 1.29 mmol) and 4-(*N*-Boc-aminomethyl)-phenylboronic acid to provide **25** as a white solid (71 mg, 279 μ mol, 22%), which was purified by flash chromatography using reverse phase C13 column eluting with a linear gradient ranging from 0 to 100% acetonitrile/water. ^1H NMR (400 MHz, D $_2$ O): δ 7.98 (s, 1H), 7.51 (s, 1H), 7.41–7.37 (m, 4H), 4.13 (s, 2H), 3.18 (s, 3H). ^{13}C NMR (100 MHz, D $_2$ O): δ 154.89, 140.05, 134.48, 132.42, 129.83, 129.43, 126.76, 115.44, 42.61, 26.54. MS (ESI) 255 m/z [$M + H$] $^+$. Purity ($\geq 98\%$, t_r = 4.32 min).

4-(1-Methyl-2-oxo-2,3-dihydro-1H-imidazo[4,5-b]pyridin-6-yl)-benzamide (**26**). The general procedure A was followed using **6** (200 mg, 421 μ mol) and 4-carbamoylphenylboronic acid to provide **26** as a white solid (54 mg, 200 μ mol, 48%). ^1H NMR (400 MHz, DMSO- d_6): δ 11.65 (s, 1H), 8.30 (d, J = 2.0 Hz, 1H), 8.04 (br, 1H), 7.98 (d, J = 8.4 Hz, 2H), 7.83 (d, J = 2.0 Hz, 1H), 7.81 (d, J = 8.8 Hz, 2H), 7.38 (br, 1H), 3.64 (s, 3H). ^{13}C NMR (100 MHz, DMSO- d_6): δ 167.47, 154.10, 143.51, 140.68, 138.36, 132.85, 128.48, 128.17, 126.25, 125.48, 112.20, 26.44. MS (ESI) 269.1 m/z [$M + H$] $^+$. Purity ($\geq 98\%$, t_r = 4.80 min).

3-(1-Methyl-2-oxo-3-trityl-2,3-dihydro-1H-imidazo[4,5-b]pyridin-6-yl)benzoic Acid (**27**). A reaction mixture of **6** (6.22 g, 13.1 mmol), phenyl boronic acid (2.81 g, 16.9 mmol), Pd $_2$ (dba) $_3$ (99 mg, 1 mol %), PCy $_3$ (108 mg, 2 mol %), and K $_3$ PO $_4$ (2 M, 12 mL) in dioxane (28 mL) was stirred under microwave heating (100 $^\circ\text{C}$) for 1 h. The palladium catalyst was removed by filtration. The filtrate was diluted with ethyl acetate (100 mL) and treated with 1 N HCl(aq) to acidify. The aqueous layer was removed, and then, the organic layer was washed with water (20 mL) and brine (20 mL). The organic layer was dried over magnesium sulfate, filtered, and concentrated in vacuo. Purification of the crude product by flash chromatography eluting with a linear gradient ranging from 25 to 100% EtOAc–hexane provided 6.76 g (99%) of **27** as a yellow solid. ^1H NMR (400 MHz, DMSO- d_6): δ 13.07 (s, 1H), 8.18 (t, J = 1.2 Hz, 1H), 8.06 (d, J = 2.0 Hz, 1H), 7.92–7.90 (m, 2H), 7.80 (d, J = 2.0 Hz, 1H), 7.56 (t, J = 8.0 Hz, 1H), 7.51 (d, J = 7.6 Hz, 6H), 7.23 (t, J = 7.6 Hz, 6H), 7.15 (d, J = 7.2 Hz, 3H), 3.34 (s, 3H). ^{13}C NMR (100 MHz, DMSO- d_6): δ 167.17, 153.32, 142.96, 137.95, 136.81, 131.59, 130.98, 129.27, 128.82, 128.53, 128.21, 127.34, 127.27, 126.23, 125.40, 112.06, 73.78, 26.84. MS (ESI) 510.4 m/z [$M - H$] $^-$. HRMS (ESI) calcd for C $_{33}$ H $_{26}$ N $_3$ O $_3$ [$M + H$] $^+$, 512.1974; found, 512.1978.

Pentafluorophenyl 3-(1-Methyl-2-oxo-3-trityl-2,3-dihydro-1H-imidazo[4,5-b]pyridin-6-yl)benzoate (**28**). To a solution of **27** (0.502 g, 0.96 mmol) and diisopropylethyl amine (0.35 mL) in dry CH $_2$ Cl $_2$ (10 mL) was added pentafluorophenyl trifluoroacetate (0.25 mL, 1.45 mmol) dropwise at 0 $^\circ\text{C}$. The mixture was stirred for 10 min, then was warmed to the ambient temperature, and stirred for 1 h. The solvent was removed under reduced pressure, and then, purification of the crude product by flash chromatography eluting with a linear gradient ranging from 6 to 50% EtOAc–hexane yielded 0.528 g (81%) of **28** as viscous yellow oil. A solution of **28** (0.1 M) in dry CH $_2$ Cl $_2$ was prepared for the following amide formation reaction and stored at room temperature. ^1H NMR (400 MHz, CDCl $_3$): δ 8.39 (t, J = 1.6 Hz, 1H), 8.22 (dt, J = 7.6, 1.2 Hz, 1H), 8.11 (d, J = 2.0 Hz, 1H), 7.87 (ddd, J = 8.0, 1.6, 0.8 Hz, 1H), 7.66–7.60 (m, 7H), 7.34 (d, J = 2.0 Hz, 1H), 7.31–7.28 (m, 6H), 7.25–7.21 (m, 3H), 3.42 (s, 3H). ^{13}C NMR (100 MHz, CDCl $_3$): δ 162.57, 154.30, 144.09, 142.85, 139.63, 138.39, 133.18, 129.79, 129.67, 129.30, 129.21, 129.06, 127.85, 127.50, 126.74, 125.45, 111.10, 75.03, 27.12. MS (ESI) 243 m/z [decomposition of trityl group, $M + H$] $^+$. HRMS (ESI) calcd for C $_{39}$ H $_{25}$ F $_5$ N $_3$ O $_3$ [$M + H$] $^+$, 678.1816; found, 678.1814.

General Procedure B for the Synthesis of the Substituted Benzamide Analogues (19, 20, and 30–53) in Scheme 3. To a solution of **28** (0.1 M) and diisopropylethyl amine (ca. 3 equiv) was added the appropriate primary amine (1.2 equiv) at 0 $^\circ\text{C}$. The reaction mixture was warmed to the ambient temperature and stirred for 1 h. The solvent was removed by reduced pressure. The crude product was diluted with ethyl acetate (30 mL) and washed with saturated aqueous NaHCO $_3$ (10 mL) and brine (10 mL). The organic layer was dried over magnesium sulfate, filtered, and concentrated in vacuo. Purification of the crude product by flash chromatography eluting with a linear gradient ranging from 25 to 100% EtOAc–hexane provided trityl protected benzamide analogues **29**. To a solution of **29** in CH $_2$ Cl $_2$ (5 mL) was added trifluoroacetic acid (1 mL) at room temperature. The reaction mixture was stirred for 30 min. After the solvent and trifluoroacetic acid were removed in vacuo, the desired product (**19**, **20**, and **30–53**) was purified by flash chromatography eluting with a linear gradient ranging from 0 to 20% MeOH/EtOAc.

N-Methyl-3-(1-methyl-2-oxo-2,3-dihydro-1H-imidazo[4,5-b]pyridin-6-yl)benzamide (**19**). The general procedure B was followed using **28** (216 mg, 318 μ mol) and methylamine to provide **19** as a white solid (86 mg, 305 μ mol, 96%). ^1H NMR (400 MHz, DMSO- d_6): δ 11.64 (s, 1H), 8.59 (d, J = 4.4 Hz, 1H), 8.29 (d, J = 2.0 Hz, 1H), 8.14 (t, J = 1.6 Hz, 1H), 7.86–7.81 (m, 3H), 7.55 (t, J = 8.0 Hz, 1H), 3.37 (s, 3H), 2.82 (d, J = 4.8 Hz, 3H). ^{13}C NMR (100 MHz, DMSO- d_6): δ 166.49, 154.11, 143.33, 138.27, 138.07, 135.29, 129.14, 129.01, 128.94, 126.10, 125.46, 125.12, 112.23, 26.43, 26.23. MS (ESI) 283.0 m/z [$M + H$] $^+$. HRMS (ESI) calcd for C $_{15}$ H $_{15}$ N $_4$ O $_2$ [$M + H$] $^+$, 283.1195; found, 283.1194. Purity ($\geq 98\%$, t_r = 5.28 min).

= 6.0 Hz, 2H), 3.37 (s, 3H). ^{13}C NMR (100 MHz, DMSO- d_6): δ 166.03, 154.08, 143.34, 139.60, 138.33, 138.15, 135.03, 129.41, 129.07, 128.90, 128.28, 127.24, 126.75, 126.30, 125.44, 125.26, 112.21, 42.66, 26.44. MS (ESI) 359 m/z [M + H] $^+$. Purity ($\geq 98\%$, t_r = 6.90 min).

3-(1-Methyl-2-oxo-2,3-dihydro-1H-imidazo[4,5-b]pyridin-6-yl)-N-(2-(pyridin-4-yl)ethyl)benzamide (41). The general procedure B was followed using a 0.1 M solution of **28** (2 mL, 200 μmol) and 4-(2-aminoethyl)pyridine to provide **41** as a white solid (64 mg, 171 μmol , 86%). ^1H NMR (400 MHz, DMSO- d_6): δ 11.65 (s, 1H), 8.71 (t, J = 5.6 Hz, 1H), 8.66 (br, 2H), 8.27 (d, J = 2.0 Hz, 1H), 8.08 (t, J = 1.6 Hz, 1H), 7.85 (dd, J = 7.6, 1.2 Hz, 1H), 7.79–7.77 (m, 2H), 7.64 (d, J = 5.6 Hz, 2H), 7.56 (t, J = 7.6 Hz, 1H), 3.63 (q, J = 6.8 Hz, 2H), 3.37 (s, 3H), 3.05 (t, J = 6.8 Hz, 2H). ^{13}C NMR (100 MHz, DMSO- d_6): δ 166.20, 154.36, 154.09, 145.52, 143.35, 138.27, 138.12, 135.08, 129.38, 129.05, 128.88, 126.12, 125.81, 125.45, 125.16, 112.18, 34.67, 26.44. MS (ESI) 374 m/z [M + H] $^+$. Purity ($\geq 98\%$, t_r = 4.98 min).

3-(1-Methyl-2-oxo-2,3-dihydro-1H-imidazo[4,5-b]pyridin-6-yl)-N-phenethylbenzamide (42). The general procedure B was followed using a 0.1 M solution of **28** (2 mL, 200 μmol) and phenethylamine to provide **42** as a white solid (63 mg, 170 μmol , 85%). ^1H NMR (400 MHz, DMSO- d_6): δ 11.64 (s, 1H), 8.68 (t, J = 5.6 Hz, 1H), 8.29 (d, J = 2.0 Hz, 1H), 8.12 (t, J = 1.6 Hz, 1H), 7.87–7.79 (m, 3H), 7.56 (t, J = 7.6 Hz, 1H), 7.33–7.18 (m, 5H), 3.52 (q, J = 6.8 Hz, 2H), 3.37 (s, 3H), 2.88 (t, J = 7.2 Hz, 2H). ^{13}C NMR (100 MHz, DMSO- d_6): δ 166.01, 154.09, 143.33, 139.51, 138.28, 138.06, 135.35, 129.22, 129.00, 128.92, 128.66, 128.33, 126.13, 126.09, 125.45, 125.17, 112.19, 40.94, 35.12, 26.44. MS (ESI) 373 m/z [M + H] $^+$. Purity (98%, t_r = 7.15 min).

N-(2-(1H-Benzo[d]imidazol-2-yl)ethyl)-3-(1-methyl-2-oxo-2,3-dihydro-1H-imidazo[4,5-b]pyridin-6-yl)benzamide (43). The general procedure B was followed using a 0.1 M solution of **28** (2 mL, 200 μmol) and 2-(1H-benzimidazol-2-yl)ethanamine hydrochloride to provide **43** as a white solid (24 mg, 57 μmol , 29%). ^1H NMR (400 MHz, DMSO- d_6): δ 11.65 (s, 1H), 8.89 (t, J = 5.6 Hz, 1H), 8.28 (d, J = 2.0 Hz, 1H), 8.14 (s, 1H), 7.86 (d, J = 7.6 Hz, 1H), 7.82–7.80 (m, 2H), 7.58–7.54 (m, 3H), 7.23 (dd, J = 6.0, 3.2 Hz, 2H), 3.79 (q, J = 6.8 Hz, 2H), 3.36 (s, 3H), 3.21 (t, J = 6.8 Hz, 2H). ^{13}C NMR (100 MHz, DMSO- d_6): δ 166.33, 158.19, 157.89, 154.10, 152.75, 143.34, 138.28, 138.07, 135.12, 129.34, 129.01, 128.88, 126.24, 125.45, 125.28, 122.41, 114.27, 112.21, 37.85, 28.37, 26.46. MS (ESI) 413 m/z [M + H] $^+$. Purity ($\geq 98\%$, t_r = 5.42 min).

3-(1-Methyl-2-oxo-2,3-dihydro-1H-imidazo[4,5-b]pyridin-6-yl)-N-(pyridin-2-ylmethyl)benzamide (44). The general procedure B was followed using a 0.1 M solution of **28** (2 mL, 200 μmol) and 2-(aminomethyl)pyridine to provide **44** as a white solid (53 mg, 148 μmol , 74%). ^1H NMR (400 MHz, DMSO- d_6): δ 11.64 (s, 1H), 9.26 (t, J = 6.0 Hz, 1H), 8.54 (d, J = 4.8 Hz, 1H), 8.32 (d, J = 5.0 Hz, 1H), 8.25 (s, 1H), 7.92–7.88 (m, 2H), 7.82–7.77 (m, 2H), 7.59 (t, J = 7.6 Hz, 1H), 7.39 (d, J = 7.6 Hz, 1H), 7.30 (dd, J = 7.2, 4.8 Hz, 1H), 4.63 (d, J = 5.6 Hz, 2H), 3.36 (s, 3H). ^{13}C NMR (100 MHz, DMSO- d_6): δ 166.25, 158.59, 154.09, 148.57, 143.36, 138.34, 138.17, 137.10, 134.87, 129.50, 129.11, 128.88, 126.34, 125.46, 125.32, 122.23, 121.19, 112.21, 44.63, 26.45. MS (ESI) 360 m/z [M + H] $^+$. Purity ($\geq 98\%$, t_r = 4.94 min).

N-((1H-Benzo[d]imidazol-2-yl)methyl)-3-(1-methyl-2-oxo-2,3-dihydro-1H-imidazo[4,5-b]pyridin-6-yl)benzamide (45). The general procedure B was followed using a 0.1 M solution of **28** (2.5 mL, 250 μmol) and (1H-benzimidazol-2-yl)methylamine hydrochloride to provide **45** as a white solid (65 mg, 164 μmol , 66%). ^1H NMR (400 MHz, DMSO- d_6): δ 11.66 (s, 1H), 9.49 (t, J = 5.2 Hz, 1H), 8.33 (d, J = 2.0 Hz, 1H), 8.29 (s, 1H), 7.93 (dd, J = 7.6, 1.6 Hz, 1H), 7.81 (d, J = 2.0 Hz, 1H), 7.68–7.60 (m, 3H), 7.36 (dd, J = 6.0, 3.2 Hz, 2H), 4.88 (d, J = 5.6 Hz, 2H), 3.37 (s, 3H). ^{13}C NMR (100 MHz, DMSO- d_6): δ 166.76, 154.09, 152.37, 143.41, 138.30, 138.15, 134.16, 129.81, 129.16, 128.76, 126.54, 125.54, 125.48, 123.66, 114.35, 112.11, 36.98, 26.45. MS (ESI) 399 m/z [M + H] $^+$. Purity (88%, t_r = 5.35 min).

3-(1-Methyl-2-oxo-2,3-dihydro-1H-imidazo[4,5-b]pyridin-6-yl)-N-(3-phenylpropyl)benzamide (46). The general procedure B was followed using a 0.1 M solution of **28** (2 mL, 200 μmol) and 3-phenylpropylamine to provide **46** as a white solid (43 mg, 111 μmol ,

56%). ^1H NMR (400 MHz, DMSO- d_6): δ 11.61 (s, 1H), 8.60 (t, J = 5.6 Hz, 1H), 8.30 (d, J = 2.0 Hz, 1H), 8.14 (t, J = 1.6 Hz, 1H), 7.86–7.82 (m, 2H), 7.80 (d, J = 2.0 Hz, 1H), 7.56 (t, J = 8.0 Hz, 1H), 7.30–7.15 (m, 5H), 3.37–3.29 (m, 5H), 2.65 (t, J = 7.6 Hz, 2H), 1.86 (p, J = 7.6 Hz, 2H). ^{13}C NMR (100 MHz, DMSO- d_6): δ 166.04, 154.10, 143.32, 141.75, 138.32, 138.07, 135.42, 129.21, 128.99, 128.97, 128.31, 128.28, 126.20, 125.73, 125.45, 125.21, 112.24, 38.96, 32.67, 30.89, 26.46. MS (ESI) 387.3 m/z [M + H] $^+$. HRMS (ESI) calcd for $\text{C}_{23}\text{H}_{23}\text{N}_4\text{O}_2$ [M + H] $^+$, 387.1821; found, 387.1818. Purity ($\geq 98\%$, t_r = 7.58 min).

N-(3-(4-Fluorophenyl)propyl)-3-(1-methyl-2-oxo-2,3-dihydro-1H-imidazo[4,5-b]pyridin-6-yl)benzamide (47). The general procedure B was followed using a 0.1 M solution of **28** (2 mL, 200 μmol) and 3-(4-fluorophenyl)propan-1-amine to provide **47** as a white solid (56 mg, 137 μmol , 69%). ^1H NMR (400 MHz, DMSO- d_6): δ 11.63 (s, 1H), 8.58 (t, J = 5.6 Hz, 1H), 8.30 (d, J = 2.0 Hz, 1H), 8.13 (t, J = 1.6 Hz, 1H), 7.86–7.80 (m, 2H), 7.80 (d, J = 2.0 Hz, 1H), 7.56 (t, J = 7.6 Hz, 1H), 7.30–7.25 (m, 2H), 7.13–7.07 (m, 2H), 3.37 (s, 3H), 3.31 (q, J = 7.2 Hz, 2H), 2.64 (t, J = 7.6 Hz, 2H), 1.84 (p, J = 7.6, 7.2 Hz, 2H). ^{13}C NMR (100 MHz, DMSO- d_6): δ 166.04, 154.09, 143.32, 138.31, 138.07, 137.85, 137.82, 135.40, 130.06, 129.98, 129.20, 128.97, 128.96, 126.18, 125.44, 125.20, 114.99, 114.79, 112.22, 38.81, 31.74, 30.93, 26.45. MS (ESI) 405.2 m/z [M + H] $^+$. HRMS (ESI) calcd for $\text{C}_{23}\text{H}_{22}\text{FN}_4\text{O}_2$ [M + H] $^+$, 405.1727; found, 405.1727. Purity ($\geq 98\%$, t_r = 7.66 min).

N-(3-(1H-Indol-3-yl)propyl)-3-(1-methyl-2-oxo-2,3-dihydro-1H-imidazo[4,5-b]pyridin-6-yl)benzamide (48). The general procedure B was followed using a 0.1 M solution of **28** (2 mL, 200 μmol) and 3-(1H-indol-3-yl)propan-1-amine hydrochloride to provide **48** as a white solid (51 mg, 119 μmol , 59%). ^1H NMR (400 MHz, DMSO- d_6): δ 11.63 (s, 1H), 10.76 (s, 1H), 8.61 (t, J = 5.6 Hz, 1H), 8.30 (d, J = 2.0 Hz, 1H), 8.15 (t, J = 1.6 Hz, 1H), 7.86–7.82 (m, 2H), 7.80 (d, J = 2.0 Hz, 1H), 7.56 (t, J = 7.6 Hz, 1H), 7.52 (d, J = 8.0 Hz, 1H), 7.33 (d, J = 8.0 Hz, 1H), 7.17 (d, J = 2.0 Hz, 1H), 7.06 (td, J = 7.2, 1.2 Hz, 1H), 6.96 (td, J = 8.0, 0.8 Hz, 1H), 3.40–3.33 (m, 5H), 2.76 (t, J = 7.2 Hz, 2H), 1.94 (p, J = 7.2 Hz, 2H). ^{13}C NMR (100 MHz, DMSO- d_6): δ 166.02, 154.09, 143.31, 138.31, 138.07, 136.32, 135.49, 129.17, 128.97, 127.13, 126.19, 125.44, 125.20, 122.27, 120.81, 118.26, 118.07, 114.00, 112.23, 111.31, 29.83, 26.45, 22.23. MS (ESI) 426.2 m/z [M + H] $^+$. HRMS (ESI) calcd for $\text{C}_{25}\text{H}_{24}\text{N}_5\text{O}_2$ [M + H] $^+$, 426.1930; found, 426.1928. Purity ($\geq 98\%$, t_r = 7.38 min).

3-(1-Methyl-2-oxo-2,3-dihydro-1H-imidazo[4,5-b]pyridin-6-yl)-N-(3-(pyridin-3-yl)propyl)benzamide (49). The general procedure B was followed using a 0.1 M solution of **28** (2 mL, 200 μmol) and 3-(pyridin-3-yl)propan-1-amine hydrochloride to provide **49** as a white solid (55 mg, 141 μmol , 71%). ^1H NMR (400 MHz, DMSO- d_6): δ 11.64 (s, 1H), 8.67–8.63 (m, 2H), 8.54 (d, J = 4.4 Hz, 1H), 8.30 (d, J = 2.0 Hz, 1H), 8.14 (s, 1H), 7.98 (d, J = 8.0 Hz, 1H), 7.86–7.82 (m, 2H), 7.80 (d, J = 2.0 Hz, 1H), 7.58–7.54 (m, 2H), 3.37–3.31 (m, 5H), 2.75 (t, J = 7.2 Hz, 2H), 1.90 (p, J = 7.2 Hz, 2H). ^{13}C NMR (100 MHz, DMSO- d_6): δ 166.12, 154.10, 146.76, 144.51, 143.33, 139.35, 138.70, 138.31, 138.08, 135.34, 129.24, 128.98, 128.95, 126.20, 125.45, 125.22, 124.58, 112.23, 38.61, 30.26, 29.48, 26.45. MS (ESI) 388.2 m/z [M + H] $^+$. Purity ($\geq 98\%$, t_r = 5.12 min).

N-(3-(1H-Imidazol-4-yl)propyl)-3-(1-methyl-2-oxo-2,3-dihydro-1H-imidazo[4,5-b]pyridin-6-yl)benzamide (50). The general procedure B was followed using a 0.1 M solution of **28** (2 mL, 200 μmol) and 3-(1H-imidazol-4-yl)propan-1-amine hydrochloride to provide **50** as a white solid (43 mg, 113 μmol , 57%). ^1H NMR (400 MHz, DMSO- d_6): δ 14.24 (br, 1H), 11.65 (s, 1H), 8.96 (d, J = 1.2 Hz, 1H), 8.70 (t, J = 5.6 Hz, 1H), 8.30 (d, J = 2.0 Hz, 1H), 8.15 (s, 1H), 7.87 (d, J = 8.0 Hz, 1H), 7.83 (d, J = 7.6 Hz, 1H), 7.81 (d, J = 1.6 Hz, 1H), 7.57 (t, J = 7.6 Hz, 1H), 7.47 (s, 1H), 3.37–3.32 (m, 5H), 2.72 (t, J = 7.2 Hz, 2H), 1.90 (p, J = 7.2 Hz, 2H). ^{13}C NMR (100 MHz, DMSO- d_6): δ 166.19, 154.10, 143.35, 138.29, 138.11, 135.22, 133.71, 133.06, 129.32, 129.03, 128.91, 126.20, 125.46, 125.18, 115.58, 112.21, 38.37, 28.03, 26.46, 21.55. MS (ESI) 377.3 m/z [M + H] $^+$. Purity (96%, t_r = 5.02 min).

N-(3-Cyclopentylpropyl)-3-(1-methyl-2-oxo-2,3-dihydro-1H-imidazo[4,5-b]pyridin-6-yl)benzamide (51). The general procedure B

was followed using a 0.1 M solution of **28** (2.0 mL, 200 μ mol) and 3-cyclopentylpropan-1-amine to provide **51** as a white solid (32 mg, 84 mmol, 42%). ^1H NMR (400 MHz, DMSO- d_6): δ 11.63 (s, 1H), 8.55 (d, $J = 5.6$ Hz, 1H), 8.29 (d, $J = 2.0$ Hz, 1H), 8.13 (d, $J = 1.6$ Hz, 1H), 7.86–7.81 (m, 2H), 7.80 (d, $J = 2.0$ Hz, 1H), 7.55 (t, $J = 7.6$ Hz, 1H), 3.37 (s, 3H), 3.28 (q, $J = 6.8$ Hz, 2H), 1.81–1.69 (m, 3H), 1.60–1.44 (m, 6H), 1.36–1.30 (m, 2H), 1.10–1.04 (m, 2H). ^{13}C NMR (100 MHz, DMSO- d_6): δ 165.86, 154.09, 143.32, 138.31, 138.06, 135.44, 129.16, 128.97, 126.17, 125.45, 125.17, 112.23, 39.37, 33.02, 32.22, 28.41, 26.45, 24.70. MS (ESI) 379.4 m/z [$M + H$] $^+$. Purity ($\geq 98\%$, $t_r = 8.39$ min).

2-(3-(1-Nethyl-2-oxo-2,3-dihydro-1H-imidazo[4,5-b]pyridin-6-yl)-benzamido)-4-phenylbutanoic Acid (52). The general procedure was followed using a 0.1 M solution of **28** (3 mL, 300 μ mol) and benzyl 2-amino-4-phenylbutanoate followed by debenzoylation using Pd/C, H_2 , and MeOH (10 mL) for 12 h at room temperature to provide **52** as a white solid (47 mg, 110 μ mol, 37% over three steps). ^1H NMR (400 MHz, DMSO- d_6): δ 12.66 (s, 1H), 11.64 (s, 1H), 8.81 (d, $J = 7.6$ Hz, 1H), 8.33 (d, $J = 2.0$ Hz, 1H), 8.21 (s, 1H), 7.90 (dt, $J = 7.6, 2.0$ Hz, 2H), 7.82 (d, $J = 2.0$ Hz, 1H), 7.60 (t, $J = 7.6$ Hz, 1H), 7.31–7.17 (m, 5H), 4.42–4.37 (m, 1H), 3.38 (s, 3H), 2.80–2.65 (m, 2H), 2.16–2.08 (m, 2H). ^{13}C NMR (100 MHz, DMSO- d_6): δ 173.70, 166.46, 154.10, 143.36, 141.06, 138.36, 138.14, 134.71, 129.61, 129.02, 128.92, 128.40, 128.33, 126.51, 125.91, 125.52, 125.47, 112.25, 52.14, 32.43, 31.84, 26.46. MS (ESI) 429.4 m/z [$M - H$] $^-$. Purity (53%/47%, $t_r = 7.00$ and 7.71 min).

2-Benzyl-3-(3-(1-methyl-2-oxo-2,3-dihydro-1H-imidazo[4,5-b]pyridin-6-yl)benzamido)propanoic Acid (53). The general procedure B was followed using a 0.1 M solution of **28** (2 mL, 200 μ mol) and methyl 3-amino-2-benzylpropanoate hydrochloride followed by hydrolysis using 10% KOH(aq) (10 mL) and MeOH (5 mL) at 60 $^\circ\text{C}$ for 12 h to provide **53** as a white solid (69 mg, 160 μ mol, 80%). ^1H NMR (400 MHz, DMSO- d_6): δ 12.30 (s, 1H), 11.65 (s, 1H), 8.73 (t, $J = 5.6$ Hz, 1H), 8.31 (d, $J = 2.0$ Hz, 1H), 8.14 (s, 1H), 7.87 (d, $J = 7.6$ Hz, 1H), 7.83 (d, $J = 8.0$ Hz, 1H), 7.80 (d, $J = 1.6$ Hz, 1H), 7.57 (d, $J = 8.0$ Hz, 1H), 7.31–7.18 (m, 5H), 3.55–3.42 (m, 2H), 3.38 (s, 3H), 3.00 (p, $J = 7.6$ Hz, 1H), 2.91–2.81 (m, 2H). ^{13}C NMR (100 MHz, DMSO- d_6): δ 174.87, 166.28, 154.10, 143.35, 139.17, 138.32, 138.07, 135.14, 129.34, 129.01, 128.91, 128.77, 128.25, 126.24, 126.17, 125.46, 125.26, 112.21, 46.74, 41.26, 35.52, 26.46. MS (ESI) 429.4 m/z [$M - H$] $^-$. HRMS (ESI) calcd for $\text{C}_{24}\text{H}_{23}\text{N}_4\text{O}_4$ [$M + H$] $^+$, 431.1719; found, 431.1724. Purity (60%/24%, $t_r = 6.66$ and 7.43 min).

General Procedure C for the Synthesis of the Substituted Benzamide Analogues (57–63) in Scheme 4. **3-(1-Methyl-2-oxo-3-trityl-2,3-dihydro-1H-imidazo[4,5-b]pyridin-6-yl)-N-(prop-2-yn-1-yl)benzamide (54)**. To a solution of **28** (0.1 M CH_2Cl_2 , 5 mL, 5.0 mmol) were added monoproprylamine hydrochloride (79 mg) and diisopropylethylamine (1.0 mL) at room temperature. The reaction mixture was stirred at 50 $^\circ\text{C}$ for 1 h. The mixture was cooled to ambient, and then, solvent was removed by evaporation. The crude mixture was diluted with ethyl acetate (40 mL) and was washed with saturated aqueous NaHCO_3 (10 mL) and brine (10 mL). The organic layer was dried over magnesium sulfate, filtered, and concentrated in vacuo. Purification of the crude product by flash chromatography eluting with a linear gradient ranging from 12 to 100% EtOAc–hexane provided 0.27 g (98%) of **54** as a white solid. ^1H NMR (400 MHz, DMSO- d_6): δ 8.99 (t, $J = 5.6$ Hz, 1H), 8.17 (d, $J = 2.0$ Hz, 1H), 8.14 (t, $J = 1.2$ Hz, 1H), 7.87–7.82 (m, 3H), 7.56–7.50 (m, 7H), 7.26–7.22 (m, 6H), 7.17–7.13 (m, 3H), 4.09 (dd, $J = 5.6, 2.4$ Hz), 3.33 (s, 3H), 3.15 (t, $J = 2.4$ Hz, 1H). ^{13}C NMR (100 MHz, DMSO- d_6): δ 165.64, 153.31, 142.95, 142.92, 137.54, 137.02, 134.41, 129.46, 129.12, 128.85, 128.53, 127.26, 126.55, 126.23, 125.36, 125.01, 111.81, 81.17, 73.78, 72.99, 28.51, 26.84. MS (ESI) 243 m/z [decomposition of trityl group, $M + H$] $^+$. HRMS (ESI) calcd for $\text{C}_{36}\text{H}_{29}\text{N}_4\text{O}_2$ [$M + H$] $^+$, 549.2291; found, 549.2297.

3-(1-Methyl-2-oxo-2,3-dihydro-1H-imidazo[4,5-b]pyridin-6-yl)-N-(3-(4-(trifluoromethyl)phenyl)propyl)benzamide (57). A mixture of **54** (0.17 g, 0.310 mmol), 1-bromo-4-(trifluoromethyl)benzene (0.110 g, 0.431 mmol), Pd(PPh $_3$) $_4$ (40 mg, 10 mol %), NEt $_3$ (0.5 mL), and CuI (5 mg) in DMF (5 mL) was stirred under heating (80 $^\circ\text{C}$) by

microwave for 1 h. The product mixture was diluted with ethyl acetate (30 mL) and washed with water (10 mL) and brine (10 mL). The combined organic layer was dried over magnesium sulfate, filtered, and concentrated in vacuo. The resulting product was purified by flash chromatography eluting with a linear gradient ranging from 25 to 100% EtOAc–hexane to afford **55a** as a pale yellow solid (0.15 g, 0.215 mmol), which was directly used for the next step. To a solution of **55a** in MeOH (10 mL) was added 10% Pd/C (ca. 30 mg) at room temperature. After air was removed from the flask using a vacuum pump, hydrogen gas was introduced using a balloon. The reaction mixture was stirred for 1 h, and the flask was evacuated under vacuum and refilled with hydrogen gas. This procedure was repeated three times, and the reaction mixture was stirred overnight at ambient temperature. Palladium on carbon was removed by filtration through a Celite pad. The filtrate was collected and evaporated to give the crude product **56a**, from which the trityl group was removed upon treatment with TFA (1 mL) in CH_2Cl_2 (10 mL) for 1 h. The TFA and solvent were then removed under reduced pressure. The resulting product was purified by flash chromatography eluting with a linear gradient ranging from 0 to 20% MeOH/EtOAc to afford **57** (67 mg, 0.148 mmol, 34% over three steps) as a white solid. ^1H NMR (400 MHz, DMSO- d_6): δ 11.64 (s, 1H), 8.61 (t, $J = 5.6$ Hz, 1H), 8.30 (d, $J = 2.0$ Hz, 1H), 8.13 (s, 1H), 7.86 (d, $J = 8.0$ Hz, 1H), 7.83 (d, $J = 8.0$ Hz, 1H), 7.80 (d, $J = 1.6$ Hz, 1H), 7.65 (d, $J = 8.0$ Hz, 2H), 7.57 (d, $J = 7.6$ Hz, 1H), 7.49 (d, $J = 8.0$ Hz, 2H), 3.38–3.31 (m, 5H), 2.76 (t, $J = 7.6$ Hz, 2H), 1.90 (p, $J = 7.2$ Hz, 2H). ^{13}C NMR (100 MHz, DMSO- d_6): δ 166.07, 154.08, 146.80, 143.32, 138.30, 138.07, 135.36, 129.21, 129.15, 129.15, 128.96, 128.94, 126.17, 125.44, 125.19, 125.10, 125.06, 112.21, 32.39, 30.46, 26.44. MS (ESI) 455 m/z [$M + H$] $^+$. HRMS (ESI) calcd for $\text{C}_{24}\text{H}_{22}\text{F}_3\text{N}_4\text{O}_2$ [$M + H$] $^+$, 455.1695; found, 455.1694. Purity ($\geq 98\%$, $t_r = 8.32$ min).

Methyl 2-(3-(3-(1-Methyl-2-oxo-2,3-dihydro-1H-imidazo[4,5-b]pyridin-6-yl)benzamido)propyl)benzoate (58). The general procedure B was followed using a 0.1 M solution of **28** (2 mL, 0.2 mmol) and methyl 2-(3-aminopropyl)benzoate hydrochloride to provide **58** as a white solid (47 mg, 0.105 mmol, 52%). ^1H NMR (400 MHz, DMSO- d_6): δ 11.63 (s, 1H), 8.65 (t, $J = 5.6$ Hz, 1H), 8.29 (d, $J = 2.0$ Hz, 1H), 8.15 (t, $J = 2.0$ Hz, 1H), 7.86–7.83 (m, 2H), 7.79 (d, $J = 2.0$ Hz, 1H), 7.65 (dd, $J = 7.6, 1.6$ Hz, 1H), 7.58–7.50 (m, 2H), 7.16 (d, $J = 7.6$ Hz, 1H), 7.01 (td, $J = 7.6, 0.8$ Hz, 1H), 4.13 (t, $J = 6.0$ Hz, 2H), 3.79 (s, 3H), 3.51 (q, $J = 6.8$ Hz, 2H), 3.36 (s, 3H), 2.02 (p, $J = 6.4$ Hz, 2H). ^{13}C NMR (100 MHz, DMSO- d_6): δ 166.25, 166.20, 157.66, 154.09, 143.31, 138.30, 138.06, 135.37, 133.51, 130.69, 129.22, 128.96, 126.22, 125.44, 125.26, 120.16, 120.09, 113.58, 112.22, 66.24, 51.75, 36.47, 28.88, 26.44. MS (ESI) 444.3 m/z [$M + H$] $^+$. Purity ($\geq 98\%$, $t_r = 7.23$ min).

N-(3-(4-(Aminomethyl)phenyl)propyl)-3-(1-methyl-2-oxo-2,3-dihydro-1H-imidazo[4,5-b]pyridin-6-yl)benzamide Hydrochloride (59). The general procedure C was followed using **54** (0.19 g, 0.349 mmol), *tert*-butyl 4-bromobenzyl carbamate (0.27, 0.94 mmol), Pd(PPh $_3$) $_4$ (40 mg, 10 mol %), NEt $_3$ (0.5 mL), and CuI (5 mg) in DMF (5 mL) to provide **55b** (0.17 g, 0.254 mmol, 73%), which was hydrogenated to give **56b** (0.12 g, 0.159 mmol, 63%). To a solution of **56b** (0.12 g, 0.159 mmol) in CH_2Cl_2 (5 mL) was added trifluoroacetic acid (ca. 1 mL). The reaction mixture was stirred for 1 h at room temperature. After evaporation of the solvent and trifluoroacetic acid, 1 N aqueous HCl was added to the product mixture. The resulting product was purified by reverse phase flash chromatography eluting with a linear gradient ranging from 5 to 100% acetonitrile–water to provide **59** (33 mg, 0.074 mmol, 46%) as a white solid. ^1H NMR (400 MHz, DMSO- d_6): δ 11.64 (s, 1H), 8.68 (t, $J = 5.6$ Hz, 1H), 8.30 (d, $J = 2.0$ Hz, 1H), 8.28 (br, 3H), 8.17 (t, $J = 1.6$ Hz, 1H), 7.87–7.83 (m, 3H), 7.56 (t, $J = 7.6$ Hz, 1H), 7.40 (d, $J = 8.0$ Hz, 2H), 7.29 (d, $J = 8.0$ Hz, 2H), 3.98 (s, 2H), 3.37 (s, 3H), 3.3–3.29 (m, 2H), 2.67 (t, $J = 7.6$ Hz, 2H), 1.86 (p, $J = 7.2$ Hz, 2H). ^{13}C NMR (100 MHz, DMSO- d_6): δ 166.04, 154.10, 143.32, 142.19, 138.29, 138.06, 135.37, 131.42, 129.20, 128.98, 128.94, 128.92, 128.57, 126.23, 125.45, 125.22, 112.28, 41.98, 32.32, 30.82, 26.48. MS (ESI) 416 m/z [$M + H$] $^+$. Purity ($\geq 98\%$, $t_r = 5.57$ min).

N-(3-(3-(Aminomethyl)phenyl)propyl)-3-(1-methyl-2-oxo-2,3-dihydro-1*H*-imidazo[4,5-*b*]pyridin-6-yl)benzamide Hydrochloride (**60**). The procedure for the synthesis of **59** was followed using **54** (144 mg, 262 μ mol) and *tert*-butyl 3-bromobenzyl carbamate to provide **60** as a white solid (35 mg, 78 μ mol, 30% over four steps). ^1H NMR (400 MHz, DMSO- d_6): δ 11.64 (s, 1H), 8.76 (t, J = 5.6 Hz, 1H), 8.35 (br, 2H), 8.31 (d, J = 2.0 Hz, 1H), 8.20 (s, 1H), 7.87–7.84 (m, 3H), 7.56 (t, J = 7.6 Hz, 1H), 7.38 (s, 1H), 7.36–7.25 (m, 3H), 3.99 (d, J = 5.2 Hz, 2H), 3.38–3.31 (m, 5H), 2.67 (t, J = 7.6 Hz, 2H), 1.89 (p, J = 7.6, 7.2 Hz, 2H). ^{13}C NMR (100 MHz, DMSO- d_6): δ 166.03, 154.10, 143.31, 142.15, 138.28, 138.05, 135.34, 133.97, 129.17, 128.99, 128.92, 128.88, 128.56, 128.43, 126.28, 126.24, 125.46, 125.21, 112.32, 42.20, 32.55, 30.72, 26.50. MS (ESI) 416 m/z [$M + \text{H}$] $^+$. Purity ($\geq 98\%$, t_r = 5.64 min).

3-(3-(3-(1-Methyl-2-oxo-2,3-dihydro-1*H*-imidazo[4,5-*b*]pyridin-6-yl)benzamido)propyl)benzoic Acid (**61**). The general procedure C were followed using **54** (153 mg, 278 μ mol) and methyl 3-bromobenzoate to provide **56d**. A solution of **56d** in MeOH (5 mL) and 10% KOH(aq) (10 mL) was stirred at 60 $^\circ\text{C}$ for 24 h. The reaction mixture was cooled to ambient, and then, 1 N HCl was added to acidify the product mixture, and a white solid precipitated. The mixture was diluted with ethyl acetate (30 mL) and washed with water (10 mL) and brine (10 mL). The organic layer was dried over magnesium sulfate, filtered, and concentrated in vacuo. Purification of the crude product by flash chromatography eluting with a linear gradient ranging from 0 to 30% MeOH/EtOAc provided **61** (26 mg, 61 μ mol, 22%, four steps). ^1H NMR (400 MHz, DMSO- d_6): δ 12.90 (br, 1H), 11.63 (s, 1H), 8.60 (t, J = 5.6 Hz, 1H), 8.30 (d, J = 1.6 Hz, 1H), 8.14 (s, 1H), 7.86–7.82 (m, 3H), 7.80 (d, J = 2.0 Hz, 1H), 7.77 (d, J = 7.6 Hz, 1H), 7.56 (t, J = 7.6 Hz, 1H), 7.48 (d, J = 7.6 Hz, 1H), 7.40 (t, J = 7.6 Hz, 1H), 3.37–3.30 (m, 5H), 2.72 (t, J = 7.6 Hz, 2H), 1.88 (p, J = 7.2 Hz, 2H). ^{13}C NMR (100 MHz, DMSO- d_6): δ 166.08, 154.09, 143.31, 142.07, 138.31, 138.07, 135.41, 129.19, 129.09, 128.96, 128.40, 128.37, 126.81, 125.44, 125.22, 112.23, 32.40, 30.77, 26.45. MS (ESI) 429 m/z [$M - \text{H}$] $^-$. Purity (95%, t_r = 6.58 min).

4-(3-(3-(1-Methyl-2-oxo-2,3-dihydro-1*H*-imidazo[4,5-*b*]pyridin-6-yl)benzamido)propyl)benzoic Acid (**62**). The procedure for the synthesis of **61** was followed using **54** (0.16 g, 0.293 mmol) and methyl 4-bromobenzoate to provide **62** as a white solid (26 mg, 60.8 μ mol, 21% over four steps). ^1H NMR (400 MHz, DMSO- d_6): δ 12.77 (br, 1H), 11.63 (s, 1H), 8.62 (t, J = 5.6 Hz, 1H), 8.30 (d, J = 2.0 Hz, 1H), 8.14 (s, 1H), 7.88–7.80 (m, 5H), 7.56 (t, J = 7.6 Hz, 1H), 7.41–7.36 (m, 2H), 3.37–3.30 (m, 5H), 2.73 (t, J = 7.6 Hz, 2H), 1.89 (p, J = 7.6 Hz, 2H). ^{13}C NMR (100 MHz, DMSO- d_6): δ 167.24, 166.05, 154.08, 147.17, 143.31, 138.30, 138.06, 135.37, 129.37, 129.19, 128.94, 128.51, 128.38, 126.18, 125.43, 125.20, 112.23, 32.60, 30.47, 26.44. MS (ESI) 429 m/z [$M - \text{H}$] $^-$. Purity ($\geq 98\%$, t_r = 6.44 min).

2-(3-(3-(1-Methyl-2-oxo-2,3-dihydro-1*H*-imidazo[4,5-*b*]pyridin-6-yl)benzamido)propyl)benzoic Acid (**63**). The procedure for the synthesis of **61** was followed using **58** (0.16 g, 0.360 mmol) to provide **63** as a white solid (0.12 g, 0.279 mmol, 78%). ^1H NMR (400 MHz, DMSO- d_6): δ 12.55 (br, 1H), 11.63 (s, 1H), 8.66 (t, J = 5.6 Hz, 1H), 8.29 (d, J = 2.0 Hz, 1H), 8.14 (s, 1H), 7.86–7.79 (m, 2H), 7.79 (d, J = 2.0 Hz, 1H), 7.64 (dd, J = 7.6, 2.0 Hz, 1H), 7.55 (d, J = 7.6 Hz, 1H), 7.48 (td, J = 8.4, 2.0 Hz, 1H), 7.13 (d, J = 8.4 Hz, 1H), 6.99 (td, J = 7.6, 0.8 Hz, 1H), 4.13 (d, J = 6.4 Hz, 2H), 3.50 (d, J = 6.4 Hz, 2H), 3.36 (s, 3H), 2.03 (p, J = 6.4 Hz, 2H). ^{13}C NMR (100 MHz, DMSO- d_6): δ 167.38, 166.22, 157.41, 154.09, 143.32, 138.31, 138.07, 135.33, 132.94, 130.63, 129.23, 128.96, 126.22, 125.44, 125.25, 121.63, 120.08, 113.53, 112.23, 66.20, 36.43, 30.66, 28.87, 26.44. MS (ESI) 429 m/z [$M - \text{H}$] $^-$. Purity ($\geq 98\%$, t_r = 6.50 min).

■ ASSOCIATED CONTENT

Supporting Information

Data collection and refinement statistics for the X-ray cocrystallization of PaTMK with **1**, **17**, and dFTM. Illustration of the four reactions that comprise the assay system. This material is available free of charge via the Internet at <http://pubs.acs.org>.

Accession Codes

Coordinates and structure factors of PaTMK complexed with **1**, **17**, and dFTM are available from the Protein Data Bank with accession codes 3UWK, 3UWO, and 3UXM, respectively.

■ AUTHOR INFORMATION

Corresponding Author

*(M.P.) Tel: 860-339-5319. Fax: 860-339-5319. E-mail: marksplummer@gmail.com. (W.R.R.) Tel: 561-228-2450. Fax: 561-228-3052. E-mail: roush@scripps.edu.

■ ACKNOWLEDGMENTS

Support by the Pfizer-Scripps Florida postdoctoral research fellow program to J.Y.C. is gratefully acknowledged. Additional financial support for J.Y.C. and W.R.R. at Scripps Florida was provided by NIH Grant U54MH084512, Hugh Rosen, Principal Investigator. We also thank Lisa Mullins and Joe Penzien of Pfizer for performing preliminary antibacterial assays.

■ ABBREVIATIONS USED

TP_{5A}, P1-(5'-adenosyl)-P5-(5'-thymidyl)pentaphosphate; dFTM, deoxy-fluorothymidine; dFTM, 5'-fluorodeoxythymidine; thiourea- α -TM, 5'-deoxy-5'-*N*-arylthiourea α -thymidine derivatives; DTBN, 5,5'-dithio-bis (2-nitrobenzoic acid); MIC, minimum inhibitory concentration; IC₅₀, half-maximal inhibitory concentration

■ REFERENCES

- (1) Payne, D. J.; Gwynn, M. N.; Holmes, D. J.; Pompliano, D. L. Drugs for bad bugs: Confronting the challenges of antibacterial discovery. *Nat. Rev. Drug Discovery* **2007**, *6* (1), 29–40.
- (2) Obritsch, M. D.; Fish, D. N.; MacLaren, R.; Jung, R. Nosocomial infections due to multidrug-resistant *Pseudomonas aeruginosa*: Epidemiology and treatment options. *Pharmacotherapy* **2005**, *25* (10), 1353–1364.
- (3) Rice, L. B. The clinical consequences of antimicrobial resistance. *Curr. Opin. Microbiol.* **2009**, *12* (5), 476–481.
- (4) Rice, L. B. Emerging issues in the management of infections caused by multidrug-resistant gram-negative bacteria. *Cleve. Clin. J. Med.* **2007**, *74* (Suppl. 4), S12–S20.
- (5) Kandeel, M.; Kato, A.; Kitamura, Y.; Kitade, Y. Thymidylate kinase: The lost chemotherapeutic target. *Nucleic Acids Symp. Ser. (Oxford)* **2009**, *53*, 283–284.
- (6) Anderson, E. Nucleoside and nucleotide kinases. In *The Enzymes*, 3rd ed.; Academic Press: New York, 1973; Vol. 8, pp 49–96.
- (7) Van Calenbergh, S. Structure-aided design of inhibitors of *Mycobacterium tuberculosis* thymidylate kinase. *Verh. K Acad. Geneesk. Belg.* **2006**, *68* (4), 223–248.
- (8) Fioravanti, E.; Adam, V.; Munier-Lehmann, H.; Bourgeois, D. The crystal structure of *Mycobacterium tuberculosis* thymidylate kinase in complex with 3'-azidodeoxythymidine monophosphate suggests a mechanism for competitive inhibition. *Biochemistry* **2005**, *44* (1), 130–137.
- (9) Gasse, C.; Douguet, D.; Huteau, V.; Marchal, G.; Munier-Lehmann, H.; Pochet, S. Substituted benzyl-pyrimidines targeting thymidine monophosphate kinase of *Mycobacterium tuberculosis*: Synthesis and in vitro anti-mycobacterial activity. *Bioorg. Med. Chem.* **2008**, *16* (11), 6075–6085.
- (10) Gasse, C.; Huteau, V.; Douguet, D.; Munier-Lehmann, H.; Pochet, S. A new family of inhibitors of *Mycobacterium tuberculosis* thymidine monophosphate kinase. *Nucleosides Nucleotides Nucleic Acids* **2007**, *26* (8–9), 1057–1061.
- (11) Vanheusden, V.; Munier-Lehmann, H.; Froeyen, M.; Busson, R.; Rozenski, J.; Herdewijn, P.; Van Calenbergh, S. Discovery of bicyclic thymidine analogues as selective and high-affinity inhibitors of

- Mycobacterium tuberculosis* thymidine monophosphate kinase. *J. Med. Chem.* **2004**, *47* (25), 6187–6194.
- (12) Vanheusden, V.; Van Rompaey, P.; Munier-Lehmann, H.; Pochet, S.; Herdewijn, P.; Van Calenbergh, S. Thymidine and thymidine-5'-O-monophosphate analogues as inhibitors of *Mycobacterium tuberculosis* thymidylate kinase. *Bioorg. Med. Chem. Lett.* **2003**, *13* (18), 3045–3048.
- (13) Kotaka, M.; Dhaliwal, B.; Ren, J.; Nichols, C. E.; Angell, R.; Lockyer, M.; Hawkins, A. R.; Stammers, D. K. Structures of *S. aureus* thymidylate kinase reveal an atypical active site configuration and an intermediate conformational state upon substrate binding. *Protein Sci.* **2006**, *15* (4), 774–784.
- (14) Byun, Y.; Vogel, S. R.; Phipps, A. J.; Carnrot, C.; Eriksson, S.; Tiwari, R.; Tjarks, W. Synthesis and biological evaluation of inhibitors of thymidine monophosphate kinase from *Bacillus anthracis*. *Nucleosides Nucleic Acids* **2008**, *27* (3), 244–260.
- (15) Andrade, C. H.; Pasqualoto, K. F.; Ferreira, E. I.; Hopfinger, A. J. 3D-Pharmacophore mapping of thymidine-based inhibitors of TMPK as potential antituberculosis agents. *J. Comput.-Aided Mol. Des.* **2010**, *24* (2), 157–172.
- (16) Cui, H.; Ruiz-Perez, L. M.; Gonzalez-Pacanowska, D.; Gilbert, I. H. Potential application of thymidylate kinase in nucleoside analogue activation in *Plasmodium falciparum*. *Bioorg. Med. Chem.* **2010**, *18* (20), 7302–7309.
- (17) Familiar, O.; Munier-Lehmann, H.; Ainsa, J. A.; Camarasa, M. J.; Perez-Perez, M. J. Design, synthesis and inhibitory activity against *Mycobacterium tuberculosis* thymidine monophosphate kinase of acyclic nucleoside analogues with a distal imidazoquinolinone. *Eur. J. Med. Chem.* **2010**, *45* (12), 5910–5918.
- (18) Frecer, V.; Seneci, P.; Miertus, S. Computer-assisted combinatorial design of bicyclic thymidine analogs as inhibitors of *Mycobacterium tuberculosis* thymidine monophosphate kinase. *J. Comput.-Aided Mol. Des.* **2011**, *25* (1), 31–49.
- (19) Andrade, C. H.; Pasqualoto, K. F.; Ferreira, E. I.; Hopfinger, A. J. Rational design and 3D-pharmacophore mapping of 5'-thiourea-substituted alpha-thymidine analogues as mycobacterial TMPK inhibitors. *J. Chem. Inf. Model.* **2009**, *49* (4), 1070–1078.
- (20) Douguet, D.; Munier-Lehmann, H.; Labesse, G.; Pochet, S. LEA3D: A computer-aided ligand design for structure-based drug design. *J. Med. Chem.* **2005**, *48* (7), 2457–2468.
- (21) Van Daele, I.; Munier-Lehmann, H.; Froeyen, M.; Balzarini, J.; Van Calenbergh, S. Rational design of 5'-thiourea-substituted alpha-thymidine analogues as thymidine monophosphate kinase inhibitors capable of inhibiting mycobacterial growth. *J. Med. Chem.* **2007**, *50* (22), 5281–5292.
- (22) Lavie, A.; Ostermann, N.; Brundiers, R.; Goody, R. S.; Reinstein, J.; Konrad, M.; Schlichting, I. Structural basis for efficient phosphorylation of 3'-azidothymidine monophosphate by *Escherichia coli* thymidylate kinase. *Proc. Natl. Acad. Sci. U.S.A.* **1998**, *95* (24), 14045–14050.
- (23) MOE; Chemical Computing Group Inc.: Montreal, 2009.10.
- (24) Bissantz, C.; Kuhn, B.; Stahl, M. A medicinal chemist's guide to molecular interactions. *J. Med. Chem.* **2010**, *53* (14), 5061–5084.
- (25) Ma, J. C.; Dougherty, D. A. The Cation-pi Interaction. *Chem. Rev.* **1997**, *97* (5), 1303–1324.
- (26) Mecozzi, S.; West, A. P. Jr.; Dougherty, D. A. Cation-pi interactions in aromatics of biological and medicinal interest: Electrostatic potential surfaces as a useful qualitative guide. *Proc. Natl. Acad. Sci. U.S.A.* **1996**, *93* (20), 10566–10571.
- (27) Dougherty, D. A. Cation-pi interactions in chemistry and biology: a new view of benzene, Phe, Tyr, and Trp. *Science* **1996**, *271* (5246), 163–168.
- (28) Michel, J.; Tirado-Rives, J.; Jorgensen, W. L. Energetics of displacing water molecules from protein binding sites: consequences for ligand optimization. *J. Am. Chem. Soc.* **2009**, *131* (42), 15403–15411.
- (29) Grivas, S.; Lindstrom, S. Palladium(0)-catalyzed phenylation of imidazo[4,5-b]pyridines. *J. Heterocycl. Chem.* **1995**, *32*, 467–471.
- (30) Savelli, F.; Boido, A.; Vazzana, I.; Sparatore, F. Tetrahydrocyclopenta[e]pyrido[3,2-b][1,4]diazepin and -cyclopenta-[e]pyrido[2,3-b][1,4]diazepine derivatives. *J. Heterocycl. Chem.* **1987**, *24*, 1709–1716.
- (31) Kudo, N.; Perseghini, M.; Fu, G. C. A versatile method for Suzuki cross-coupling reactions of nitrogen heterocycles. *Angew. Chem., Int. Ed. Engl.* **2006**, *45* (8), 1282–1284.
- (32) Barder, T. E.; Walker, S. D.; Martinelli, J. R.; Buchwald, S. L. Catalysts for Suzuki-Miyaura coupling processes: Scope and studies of the effect of ligand structure. *J. Am. Chem. Soc.* **2005**, *127* (13), 4685–4696.
- (33) Arvela, R. K.; Leadbeater, N. E. Suzuki coupling of aryl chlorides with phenylboronic acid in water, using microwave heating with simultaneous cooling. *Org. Lett.* **2005**, *7* (11), 2101–2104.
- (34) Leadbeater, N. E. Fast, easy, clean chemistry by using water as a solvent and microwave heating: the Suzuki coupling as an illustration. *Chem. Commun. (Cambridge)* **2005**, *23*, 2881–2902.
- (35) *Glide 5.5*; Schrodinger Inc.: New York.
- (36) *Maestro9.0*; Schrodinger Inc.: New York.
- (37) Lavie, A.; Konrad, M.; Brundiers, R.; Goody, R. S.; Schlichting, I.; Reinstein, J. Crystal structure of yeast thymidylate kinase complexed with the bisubstrate inhibitor P1-(5'-adenosyl) P5-(5'-thymidyl) pentaphosphate (TP5A) at 2.0 Å resolution: Implications for catalysis and AZT activation. *Biochemistry* **1998**, *37* (11), 3677–3686.
- (38) Cabeen, M. T.; Jacobs-Wagner, C. Bacterial cell shape. *Nat. Rev. Microbiol.* **2005**, *3* (8), 601–610.
- (39) Ostermann, N.; Schlichting, I.; Brundiers, R.; Konrad, M.; Reinstein, J.; Veit, T.; Goody, R. S.; Lavie, A. Insights into the phosphoryltransfer mechanism of human thymidylate kinase gained from crystal structures of enzyme complexes along the reaction coordinate. *Structure* **2000**, *8* (6), 629–642.
- (40) Biswas, S.; Mohammad, M. M.; Patel, D. R.; Movileanu, L.; van den Berg, B. Structural insight into OprD substrate specificity. *Nat. Struct. Mol. Biol.* **2007**, *14* (11), 1108–1109.
- (41) Mach, T.; Neves, P.; Spiga, E.; Weingart, H.; Winterhalter, M.; Ruggerone, P.; Ceccarelli, M.; Gameiro, P. Facilitated permeation of antibiotics across membrane channels—Interaction of the quinolone moxifloxacin with the OmpF channel. *J. Am. Chem. Soc.* **2008**, *130* (40), 13301–13309.
- (42) Nikaido, H.; Thanassi, D. G. Penetration of lipophilic agents with multiple protonation sites into bacterial cells: tetracyclines and fluoroquinolones as examples. *Antimicrob. Agents Chemother.* **1993**, *37* (7), 1393–1399.
- (43) Carter, J. C. W.; Sweet, R. M. *Macromolecular Crystallography*, part A; Academic Press: New York, 1997; Vol. 276, pp 307–326.
- (44) The CCP4 suite: Programs for protein crystallography. *Acta Crystallogr., Sect. D: Biol. Crystallogr.* **1994**, *50* (Part 5), 760–763.
- (45) Murshudov, G. N.; Vagin, A. A.; Dodson, E. J. Refinement of macromolecular structures by the maximum-likelihood method. *Acta Crystallogr., Sect. D: Biol. Crystallogr.* **1997**, *53* (Part 3), 240–255.
- (46) Brunger, A. T. Free R value: A novel statistical quantity for assessing the accuracy of crystal structures. *Nature* **1992**, *355* (6359), 472–475.
- (47) Read, R. J. Improved fourier coefficients for maps using phases from partial structures with errors. *Acta Crystallogr., Sect. A* **1986**, *42*, 140–149.
- (48) Emsley, P.; Cowtan, K. Coot: Model-building tools for molecular graphics. *Acta Crystallogr., Sect. D: Biol. Crystallogr.* **2004**, *60* (Part 12, Part 1), 2126–2132.
- (49) Read, R. J. Pushing the boundaries of molecular replacement with maximum likelihood. *Acta Crystallogr., Sect. D: Biol. Crystallogr.* **2001**, *57* (Part 10), 1373–1382.
- (50) Bricogne, G.; Blanc, E.; Brandl, M.; Eflensburg, C.; Keller, P.; Paciorek, W.; Roversi, P.; Smart, O.; Vonrhein, C.; Womack, T. BUSTER, version 2.8.0; Global Phasing Ltd.: Cambridge, United Kingdom, 2009.
- (51) Petit, C. M.; Koretke, K. K. Characterization of *Streptococcus pneumoniae* thymidylate kinase: Steady-state kinetics of the forward

reaction and isothermal titration calorimetry. *Biochem. J.* 2002, 363 (Part 3), 825–831.